Applied Catalysis B: Environmental 340 (2024) 123183

Contents lists available at ScienceDirect

Applied Catalysis B: Environmental

journal homepage: www.elsevier.com/locate/apcatb

Highly efficient activation of peracetic acid via zero-valent iron-copper bimetallic nanoparticles (nZVIC) for the oxidation of sulfamethazine in aqueous solution under neutral condition

Junyang Xiao [a,b], Yangju Li [a,b], Haoran Dong [a,b,*], Zijun Pang [c], Mengxi Zhao [a,b], Daofen Huang [a,b], Jie Dong [a,b], Long Li [a,b]

[a] College of Environmental Science and Engineering, Hunan University, Changsha, Hunan 410082, China
[b] Key Laboratory of Environmental Biology and Pollution Control (Hunan University), Ministry of Education, Changsha, Hunan 410082, China
[c] School of Environment and Energy, South China University of Technology, Guangzhou, Guangdong 510006, China

ARTICLE INFO

Keywords:
Zero-valent iron-copper bimetallic nanoparticles
Peracetic acid
Sulfamethazine
Density functional theory (DFT) calculation
Advanced oxidation process

ABSTRACT

Herein, zero-valent iron-copper bimetallic nanoparticles were firstly applied to efficiently activate peracetic acid (PAA) for the removal of sulfamethazine (SMT) under neutral condition. Compared with the system of nano zero-valent iron (nZVI)-activated PAA, nZVIC/PAA system could significantly increase the removal efficiency of SMT by 70.8% at pH 7.0. It was demonstrated that the doped Cu could greatly accelerated Fe^{2+}/Fe^{3+} cycle on the surface of the nZVIC and triggered the interaction between iron and copper. $CH_3C(O)OO^{\bullet}$ and $^1O_2$ acted a dominant role on SMT removal in the nZVIC/PAA system. The transformation pathways of SMT were inferred based on DFT theory calculations and determined intermediates, and the luminescent bacteria test and toxicity prediction of degradation intermediates showed that the biotoxicity of SMT was reduced during degradation. Finally, based on the results of the practicability evaluation, the proposed nZVIC/PAA process is a promising approach for the rapid decontamination of antibiotic-polluted water.

1. Introduction

With the prosperity of society and the development of economy, the use of antibiotics has been increasing rapidly in recent decades. Sulfamethazine (SMT), a emblematical sulfonamide antibiotic, has been universally applied in human and/or livestock, and it was frequently monitored in groundwater, wastewater, and surface water [1]. Nevertheless, the conventional sewage treatment processes could not effectively eliminate antibiotics from water bodies [2]. Meanwhile, some studies have shown that these antibiotics in the environment would lead a larvaceous menaces to human life and health in the long run [3]. During the latest several decades, advanced oxidation processes (AOPs) have become an attractive way to achieve high-efficiency elimination of non-biodegradable antibiotics by generating reactive oxygen species (ROS) with strong oxidizing ability, such as singlet oxygen ($^1O_2$), superoxide radical ($O_2^{\bullet-}$), hydroxyl radical ($^{\bullet}OH$), sulfate radical ($SO_4^{\bullet-}$), and organic radicals (R-O$^{\bullet}$, e.g., acetoxyl radical ($CH_3C(O)O^{\bullet}$), acetylperoxy radical ($CH_3C(O)OO^{\bullet}$), and etc.) [4–6]. These ROS were commonly generated by means of activating the peroxides, such as hydrogen peroxide (H_2O_2), ozone (O_3), peroxymonosulfate (PMS), peroxydisulfate (PDS), peracetic acid (PAA) and so on [7].

PAA is a strong oxidizing agent with a high standard redox potential (E^0 = 1.06–1.96 V) [8], which is comparable to that of H_2O_2 (E^0 = 1.80 V) [9]. In addition, PAA has a lower O-O bond energy (159 kJ mol^{-1}) compared to some commonly utilized oxidants (e.g., H_2O_2 (213 kJ mol^{-1}) and PMS (317 kJ mol^{-1})) [10], which demonstrates that the requirement of a lower amount of energy to achieve PAA activation process [11]. Therefore, PAA-based AOPs have attracted more and more attention in research and applications owing to their higher efficiency, low toxicity, less pH-dependence, and less toxic disinfection byproducts formation potential [12]. Hitherto, there are numerous reports on PAA activation to produce ROS, mainly including UV/solar light irradiation, metal catalysis, or carbon-based catalysts [9]. Among them, metal-based (e.g., Mn^{2+}, Fe^{2+}, Cu^{2+}, and Co^{2+}) catalysts usually have better catalytic activity than other approaches, which has become a hotspot in the field of PAA activation on account of it does not require extra energy [8,13]. Fe^{2+} has been extensively employed to activate peroxides in water treatment for the elimination of refractory organic micro-pollutants

* Corresponding author at: College of Environmental Science and Engineering, Hunan University, Changsha, Hunan 410082, China.
E-mail address: dongh@hnu.edu.cn (H. Dong).

https://doi.org/10.1016/j.apcatb.2023.123183
Received 26 June 2023; Received in revised form 13 August 2023; Accepted 16 August 2023
Available online 18 August 2023

owing to its high efficiency, cost-effectiveness, and environmental benignancy [14]. Earlier, Kim et al. reported that Fe^{2+} could effectively activated PAA to produce ROS for the oxidation of micropollutants [15]. Nevertheless, the reduction efficiency of Fe^{3+} to Fe^{2+} by PAA is four orders of magnitude slower than Fe^{2+}-activated PAA, which means that a high dose of Fe^{2+} is needed to ensure the high efficiency operation of the Fe^{2+}/PAA system [5].

For the past few years, nano zero-valent iron (nZVI) has been widely utilized as a substitute for Fe^{2+} because of its simple synthesis, environmentally benign, and it enables the release of Fe^{2+} continuously as an iron source through corrosion reaction (Eqs. (1) and (2)) [16]. Zhang and his co-authors constructed nZVI/PAA system to remove tetracycline (TC), and the experimental results showed that there was an excellent TC removal efficiency from 92.9% to 100.0% in the pH range of 3.5–6.0 [17]. Unfortunately, nZVI would appear surface passivation under neutral and/or alkaline conditions, which would affect the sustainability of the reaction system [18]. For the benefit of improving the stability and catalytic reactivity of nZVI-AOPs, researchers have paid extensive attention to the various efforts for the modification of nZVI (e.g., sulfurization, surface coating, supporting materials, and bimetallic doping) [19]. Bimetallic doping modification was considered to be an effective technique to avoid passivation of nZVI under neutral alkaline conditions. Owing to the previous studies have demonstrated that Co can activate PAA more effectively than other transition metals, the current modification of nZVI in PAA-AOPs was mainly focused on Fe-Co bimetallic [9]. Earlier, Yang et al. utilized Co@mZVI to promote the activation of PAA to efficiently degrade sulfamethoxazole [2]. Xie et al. reported using the synergic effect of Co and Fe in CoFe-LDH to activate PAA for efficient degradation of pharmaceuticals in hospital wastewater [20]. Nevertheless, the entry of Co ions into the aqueous environment would have the potential toxicity for the microorganisms, and the price of Co was also expensive [2]. Cu is also a kind of the transition metals, but it is cheaper and more readily available than Co. Zhang et al. reported the removal of diclofenac (DCF) by activating PAA with zero-valent copper (ZVC) at pH 3.0 [21]. It has been demonstrated that both Fe and Cu ions occupied a catalytic ability for the activation of PAA. Besides, our research team has revealed that the zero-valent iron-copper bimetallic nanoparticles (nZVIC)-activated sulfite system had a better removal efficiency for SMT removal than the nZVI/sulfite system [18]. This was because that the addition of Cu could not only avoid the passivation of nZVI surface, but also effectively improved the Fe^{3+}/Fe^{2+} cycle, which greatly improved the catalytic activity of nZVIC. Furthermore, the ROS produced in nZVIC/PAA system may be different from and more abundant than those produced in nZVI/PAA and/or ZVC/PAA systems alone, and the bimetallic synergistic effect may occur during the activation of PAA by nZVIC to enhance the removal of pollutants by the system. Nevertheless, it is not clear that the mechanism of bimetallic-enhanced PAA activation to remove organic micropollutant in terms of the critical role of the incorporation of a second metal Cu in boosting Fe activity and whether the nZVIC/PAA system could be used under neutral conditions.

$$Fe^0 + H_2O + 1/2\ O_2 \rightarrow Fe^{2+} + 2OH^- \quad (1)$$

$$Fe^0 + 2\ H_2O \rightarrow Fe^{2+} + 2OH^- + H_2 \quad (2)$$

In the present work, nZVIC was prepared by displacement method [18], and nZVIC/PAA system was constructed to degrade SMT in aqueous solution under neutral condition. The primary purposes of this study were as follows: (i) evaluate the feasibility of nZVIC/PAA system on the removal of SMT under neutral condition; (ii) identify the principal reactive species responsible for SMT oxidation and PAA activation mechanism; (iii) explore the degradation pathways via Density Functional Theory (DFT) calculation and LC-MS analysis, and evaluate the variation of toxicity of SMT and its degradation intermediates; (iv) investigate the effects of critical parameters (e.g., Fe/Cu mass ratio, nZVIC dose, PAA concentration, and initial pH), coexisting substance in water (e.g., Cl^-, SO_4^{2-}, HCO_3^-, and humic acid) on the removal of SMT; (v) examine the applicability of nZVIC/PAA process in different water matrix (e.g., river water, groundwater, and tap water), the ability to degrade other pollutants, and the reusability of nZVIC.

2. Methods and materials

2.1. Chemical reagents

The compounding of PAA stock solution (>15% PAA) mainly including the reaction of I solution and II solution for approximately 48 h at 25.0 °C in the dark place, and then preserved at 4.0 °C. The solutions of I and II were all provided by Guanghua Sci-Tech Co., Ltd. (Guangdong, China). The concentrations of PAA and coexisting H_2O_2 in the PAA stock solution were standardized by the iodometric titration method (GB/T19104–2021, China), and the molar ratio of [PAA]/[H_2O_2] in the PAA stock solution was about 1.8. The residual concentration of PAA in the nZVIC/PAA system was measured via our previously-reported iodometric spectrophotometry [22]. PAA was unstable at low concentrations and may decompose to form acetic acid (HAc) and H_2O_2 [23], the concentration change of selected 0.2 mM PAA in ultrapure water over a reaction time of 20 min was monitored (Fig. S1). The results showed that the concentration of PAA did not change significantly within 20 min. Sulfamethazine ($C_{12}H_{14}N_4O_2S$, SMT, ≥99%) was acquired from Yien Chemical Technology Co., Ltd (Shanghai, China). Sodium borohydride ($NaBH_4$, ≥98%) was obtained from Comeo Chemical Reagent Co., Ltd (Tianjin, China). Ferric chloride hexahydrate ($FeCl_3$·6 H_2O, ≥99%) and copper sulfate pentahydrate ($CuSO_4$·5 H_2O, AR) were purchased from Sinopharm Chemical Reagent Co., Ltd (Shanghai, China). The other chemicals and reagents utilized in the present study were listed in **Text S1** in the Supporting Information (SI).

2.2. Synthesis of the catalysts

The catalysts of nZVI and nZVIC were fabricated through a sodium borohydride reduction method and a displacement method, respectively, based on our previous work with some modifications [18]. For the synthesis of the nZVI, first of all, 300 mL of $FeCl_3$·6 H_2O (50.0 mM) was added to a 1000 mL three-neck flask with continuous aerating of N_2 into the solution for 30 min. Then, the $NaBH_4$ solution with the same volume was added dropwise into the above solution at a constant speed through a peristaltic pump (Shenchen , Shanghai , China) under continuous stirring. After the completion of solution dropping, the mixed solution was stirred again for 30 min to allow the solution fully react. After that, the generated precipitate was filtered and washed more than three times with ethanol, and dried in a vacuum drying oven at 60.0 °C for at least 12 h. The black solid collected after drying was noted as nZVI.

For the synthesis of the nZVIC, the process was based on the synthesis of nZVI with a displacement method. Briefly, the above synthesized nZVI was added to the beaker with different concentrations of $CuSO_4$·5 H_2O solution and reacted for around 20 min during mechanical stirring. Then, the solids in the beaker were magnetically separated, washed and dried as mentioned above. The solid collected after drying was noted as nZVIC. The theoretical Cu loading in the nZVIC was controlled by adjusting the concentration of $CuSO_4$ solution. The fabricated nZVI and nZVIC were collected in a centrifuge tube and stored at 4.0 °C to avoid rapid oxidation before the reaction.

2.3. Experimental procedures

The implementation of all batch experiments were in the 250 mL glass bottles placed in a constant temperature shaker (TP80C, Jinlan, Shanghai) under the rate of 250 rpm at 25.0 ± 0.5 °C for a reaction of 20 min. Firstly, a predetermined amount of target pollutants was dispensed into the glass bottle. After that, a desired amount of PAA stock solution

was put into the above mentioned aqueous solution, and then regulating the initial pH to 7.0 immediately by adjunction of 1.0 M of H_2SO_4 and/or NaOH and measured with a pH-meter (PB-10, Sartorius, Germany). Lastly, the oxidation reaction was triggered by adding a certain amount of catalysts into the working aqueous solution. Samples aliquots (1 mL) were collected from the glass bottle at predetermined time intervals, filtered through a 0.22 μm PES filter and added to a liquid phase vial pre-spiked with excess sodium thiosulfate (0.1 M) for analysis of SMT or other contaminants.

2.4. Analytical methods

In order to determine the residual concentration of SMT and other pollutants during the degradation reaction in this study, a high-performance liquid chromatography (HPLC, 1200, Agilent, USA) equipped with a UV detector and a Poroshell 120 EC-C18 column (4.6 mm × 150 mm) was conducted. The analytical methods of the tested SMT and other pollutants were listed in Table S2. The analysis process of SMT degradation intermediate products by a liquid chromatography-triple quaternary rod tandem mass spectrometer (LC-MS, 6470 Triple Quad, Agilent, USA) was similar to our previous work [7]. The leaching concentration of copper in the degradation system was analyzed with an Inductively Couples Plasma-mass Spectrometer (ICP-MS, NexION 300, PerkinElmer, USA). The toxicity of SMT and its degradation intermediates were divined via quantitative structure-activity relationship (QSAR) by using Toxicity Estimation Software Tool (T.E.S.T.) (version 5.1.2). The acute toxicity of SMT degradation in the nZVIC/PAA system was assessed based on the standard method (UNE-EN-ISO 11348–3:2007 (E)) by employing the BioFixLumi luminescent bacteria as an indicator. The details of other analytical methods in the present study were represented in Text S2 of the SI.

2.5. Characterizations

The X-ray powder diffraction patterns of the nZVI and nZVIC were carried out via an X-ray diffractometer (XRD, Bruker D8 Advance, Germany) equipped with Cu Kα radiation. An X-ray photoelectron spectrometry (XPS, Thermo Escalab 250XI, USA) was applied to scrutinize the surface compositions and changes of the chemical state of nZVIC before and after degradation reaction. The morphological structure characteristics of nZVIC was confirmed via a Scanning Electron Microscope Equipped with an Energy Dispersive Spectrometer (SEM-EDS, FEI-QUANTA250, USA). The electrochemical impedance spectroscopy (EIS) and Tafel polarization curves of the synthesized nZVI and nZVIC were executed with an electrochemical workstation (CHI760E, CH Instrument Co., Shanghai, China) with a conventional three-electrode cell system.

3. Results and discussion

3.1. Characterization of synthesized catalysts

The crystallographic and phase structures of the original and used nZVIC were examined by XRD patterns. As observed from Fig. S2, the original nZVIC not only had a diffraction peak at 44.6° belonging to Fe^0 (JCPDS No. 36–0696) [24], but also showed two diffraction peaks at 50.4° and 74.1°, which were along with the standard diffraction pattern of Cu^0 (JCPDS No. 04–0836) [25], indicating that the synthesized nZVIC mainly existed in the form of zero-valent iron and zero-valent copper. Also, there was no new diffraction peak appeared in the XRD pattern of the used nZVIC compared with the original nZVIC, indicating that the composition of the nZVIC did not change after the reaction, which was beneficial to the recycling of the material to activate PAA. In order to observe the surface morphologies of the materials, the nZVI and nZVIC before and after the reaction were characterized by means of SEM. As displayed in Fig. S3**(a)**, SEM image of raw nZVI showed a smooth spherical structure. Compared with fresh nZVI, the original nZVIC had a rough surface with some slight bulges (Fig. S3**(b)**). This phenomenon may be owing to the loading of Cu on the nZVI surface, and corresponding with the previous report [18]. As illustrated in Fig. S4, the EDS elemental mapping image demonstrated that the synthesized nZVIC was composed of two elements of Fe and Cu. In addition, the weight ratios of Fe and Cu were 71.6% and 28.4%, respectively, which was close to the theoretical value of 3:1 (Fig. S5). Furthermore, the XPS spectra showed that the synthesized nZVIC contained Cu element (Fig. S6). The detection of Cu element in EDS and XPS analysis further revealed the successful loading of Cu on the nZVIC surface. Figs S7 displayed the SEM images of the used nZVI and nZVIC, which appeared some lamellar structures in addition to the spherical structures, indicating that the raw nZVI and nZVIC were corroded during the reaction to form iron and/or copper (oxy) hydroxide. However, the used nZVIC had less lamellar structure compared with the used nZVI, which might be due to the presence of Cu element that could alleviate the passivation of nZVI during the reaction.

3.2. Evaluating the performance of nZVIC/PAA system

The different reaction systems (nZVIC, PAA, nZVIC/H_2O_2, nZVI/PAA, and nZVIC/PAA) for the removal of SMT at initial pH of 7.0 were conducted, and the results were illustrated in Fig. 1. For PAA alone process, the removal efficiency of SMT was only 1.9% after reaction within 20 min, which indicated that PAA alone had a weak oxidation ability to SMT. Intriguingly, the SMT removal efficiency reached 10.7% in the nZVIC reaction system, which might be due to the low adsorption or activation of molecular oxygen by nZVIC in aqueous (Eqs. (3–6)) [26, 27]. Additionally, when nZVI was utilized as an activator for PAA, the removal efficiency of SMT could be attained to 20.6%. It was gratifying to note that the removal efficiency of SMT was considerably improved in the nZVIC activated PAA system (nZVIC/PAA), reaching 91.4% within 20 min of reaction. Simultaneously, because of the existence of H_2O_2 in PAA solution, the SMT removal by nZVIC/H_2O_2 system (the concentration of H_2O_2 is equal to the coexistent H_2O_2 in PAA solution) was studied. The removal efficiency of SMT in nZVIC/H_2O_2 system was only 10.6% after 20 min, which indicated that PAA operated a primary role in the removal of SMT in nZVIC/PAA system. The elimination of SMT in the nZVIC/PAA system followed pseudo-first-order kinetics with k_{obs} (**Eq. (S1)**) of 0.1304 min^{-1}, which was superior to the other reaction systems (0.0004 min^{-1}, 0.0036 min^{-1}, 0.0088 min^{-1}, and 0.0037 min^{-1} for PAA, nZVIC, nZVI/PAA, and nZVIC/H_2O_2, respectively) (Fig. S8). In

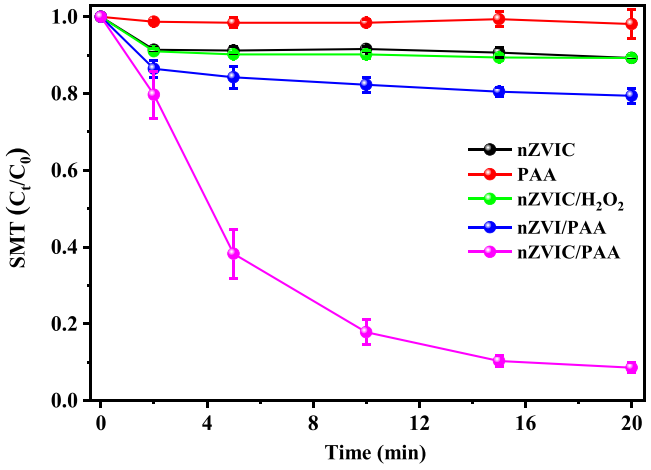

Fig. 1. The degradation of SMT in different reaction systems. Reaction conditions: $[SMT]_0$ = 10.0 μM, $[nZVIC]_0$ = $[nZVI]_0$ = 50.0 mg L^{-1}, $[PAA]_0$ = 0.2 mM, $[coexistent\ H_2O_2]_0$ = 0.11 mM, pH_0 = 7.0 ± 0.1, and T = 25 ± 0.5 °C.

addition, the decomposition of PAA in the different reaction systems within 20 min was also studied. As observed from Fig. S9, PAA hardly decomposed in PAA alone system within 20 min, which was consistent with the experimental phenomenon that PAA alone cannot effectively degrade SMT. Nevertheless, PAA was decomposed in the presence of nZVI and nZVIC, and the decomposition was more significant in the presence of nZVIC. This phenomenon indicated that both nZVI and nZVIC could activate PAA to produce ROS for the degradation of SMT, and nZVIC had a better activation effect on PAA than that of nZVI. Furthermore, the leaching concentrations of total iron (total copper) and Fe^{2+} (Cu^{+}) in the nZVIC/PAA system were measured (Figs. S10-S11). As the reaction proceeds, the leaching concentrations of total iron and total copper increased gradually, and the ferrous iron increased first and then decreased. It was discovered that the leaching concentrations of total iron and total copper in nZVIC/PAA system were less than 0.46 mg L^{-1} and 0.16 mg L^{-1}, respectively, which met the relevant requirements of the Environmental Quality Standards for Surface Water (GB 3838–2002, China) and Standards for Drinking Water Quality (GB 5749–2022, China). In order to explore the effect of leaching iron and copper ions on the activation of PAA, the removal of SMT in Fe^{2+}/PAA and Cu^{2+}/PAA systems were investigated. As demonstrated in Fig. S12, the removal efficiency of SMT was less than 15.0% in both homogeneous systems, which indicated that heterogeneous activation of PAA by nZVIC was dominant.

$$2Cu^0 + O_2 + 2H_2O \rightarrow 2Cu^+ + 2H_2O_2 + 2OH^- \quad (3)$$

$$Fe^0 + O_2 + 2H^+ \rightarrow Fe^{2+} + H_2O_2 \quad (4)$$

$$Cu^+ + H_2O_2 \rightarrow Cu^{2+} + {}^{\bullet}OH + OH^- \quad (5)$$

$$Fe^{2+} + H_2O_2 \rightarrow Fe^{3+} + {}^{\bullet}OH + OH^- \quad (6)$$

3.3. Mechanism of SMT elimination in reaction system

3.3.1. Identification of main ROS in nZVIC/PAA system

In accordance with the previous studies, the reactive species involved in PAA-based AOPs may include $^{\bullet}OH$ and R-$O^{\bullet}$ (for example, $CH_3C(O)O^{\bullet}$, $CH_3C(O)OO^{\bullet}$, $CH_3(O)O^{\bullet}$, and $^{\bullet}CH_3$) (Eqs. (1–16)) [2, 28–30]. In order to investigate the role of the radicals in the removal of

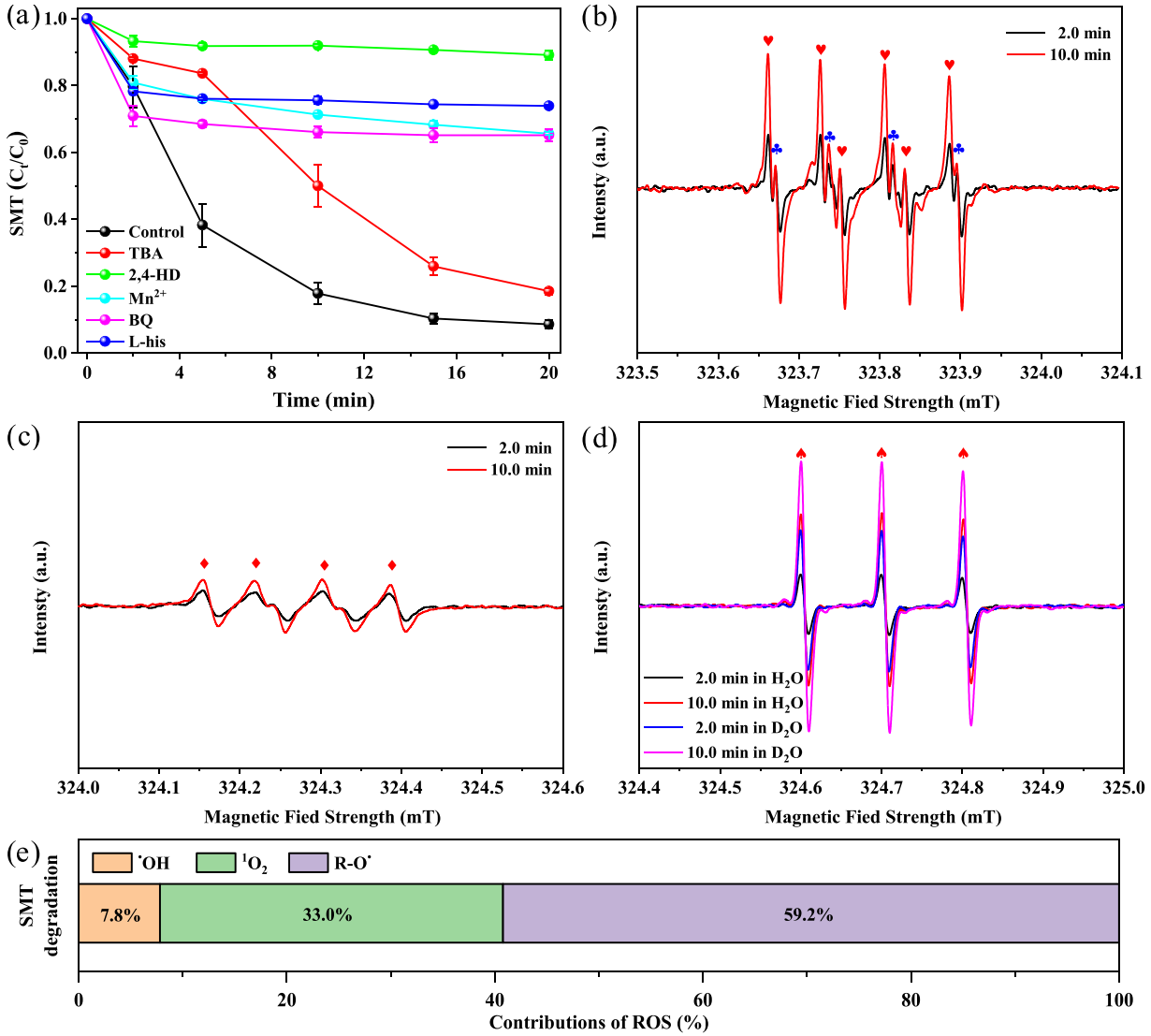

Fig. 2. (a) Effect of TBA, 2,4-HD, Mn^{2+}, BQ, and L-his on the degradation of SMT. ESR spectrum of (b) DMPO-R-$O^{\bullet}$ (♥), DMPO-$^{\bullet}OH$ (♣), (c) DMPO-$O_2^{\bullet-}$ (◆), and (d) TEMP-$^1O_2$ (♠) adducts. (e) Contributions of ROS on SMT degradation in the nZVIC/PAA system. Reaction conditions: $[SMT]_0$ = 10.0 μM, $[nZVIC]_0$ = 50.0 mg L^{-1}, $[PAA]_0$ = 0.2 mM, $[TBA]_0$ = 200.0 mM, $[2,4\text{-HD}]_0$ = 4.0 μM, $[Mn^{2+}]_0$ = 1.0 mM, $[BQ]_0$ = 1.0 mM, $[L\text{-his}]_0$ = 2.0 mM, $[DMPO]_0$ = 50.0 mM (only for b and c), $[TEMP]_0$ = 40.0 mM (only for d), pH_0 = 7.0 ± 0.1, and T = 25.0 ± 0.5 °C.

SMT in nZVIC/PAA system, radical quenching experiments were performed. As shown in Fig. 2**(a)**, the removal efficiency of SMT decreased from 91.4% to 81.5% with the addition of TBA ($k_{\bullet OH/TBA} = 6.0 \times 10^8$ M^{-1} s^{-1}) [31], and the corresponding k_{obs} value diminished from 0.1304 min^{-1} to 0.0894 min^{-1} (Fig. S13), suggesting that $^{\bullet}OH$ was present in the nZVIC/PAA system. To verify the contribution of R-O$^{\bullet}$ to SMT removal, 2,4-HD was added to the reaction system as it was a quencher for R-O$^{\bullet}$ ($k_{R\text{-}O\bullet/2,4\text{-}HD} > 5.0 \times 10^8$ M^{-1} s^{-1}) and $^{\bullet}OH$ ($k_{\bullet OH/2,4\text{-}HD} \approx 1.0 \times 10^{10}$ M^{-1} s^{-1}) [32]. Fig. 2**a** showed that 80.6% elimination of SMT was suppressed relative to the control system in the presence of 2,4-HD, substantiating the significant effect of R-O$^{\bullet}$ on SMT removal in the nZVIC/PAA system. The self-decomposition of $CH_3C(O)O^{\bullet}$ could produce $^{\bullet}CH_3$ with k of 2.3×10^5 M^{-1} s^{-1}, and the formed $^{\bullet}CH_3$ would react rapidly with O_2 to generate $CH_3(O)O^{\bullet}$ ($k_{\bullet CH3/O2} = 4.1 \times 10^9$ M^{-1} s^{-1}) (Eqs. (13–14)) [33]. In the interest of uncovering the contribution of $CH_3(O)O^{\bullet}$ and $^{\bullet}CH_3$ to the elimination of SMT in nZVIC/PAA system, the supplementary experiment was conducted under the deoxygenated condition by purging with N_2 [6]. As shown in Fig. S14, the purging of N_2 showed an ignoring impact on the removal of SMT, indicating that the contribution of $CH_3(O)O^{\bullet}$ and $^{\bullet}CH_3$ to SMT degradation could be negligible. It has been reported that Mn^{2+} could be employed as a individual scavenger for $CH_3C(O)OO^{\bullet}$ in the PAA-based AOPs (Eq. (17)) [34]. The removal efficiency of SMT decreased from 92.1% to 34.6% in the presence of Mn^{2+}. This result demonstrated that $CH_3C(O)OO^{\bullet}$ was the major radical for SMT removal in the nZVIC/PAA system. Moreover, according to the previous studies, $O_2^{\bullet-}$ may be also existed in the nZVIC/PAA system according to Eqs. (18–19) [35]. The elimination of SMT was marked declined from 91.4% to 34.8% upon addition of BQ, which was a typical inhibiting agent for $O_2^{\bullet-}$ ($k = 0.9$–1.0×10^9 M^{-1} s^{-1}) [36]. This may intimate the momentous role of $O_2^{\bullet-}$ in SMT removal of the nZVIC / PAA system, while considering the redox potential of $O_2^{\bullet-}$ was extremely low ($E^0 = -0.33$ V) [37], it was theoretically difficult for $O_2^{\bullet-}$ to directly act on the removal of SMT in the nZVIC/PAA system. It was possible that the generated $O_2^{\bullet-}$ was rapidly converted to $^1O_2$, which played an indirect role in the degradation of SMT (Eqs. (20–25)) [6,38,39].

It has been reported that $^1O_2$ could be formed through the spontaneous decomposition of PAA via the attack of central C atom by peroxy-group (Eq. (26)) [40]. As illustrated in Fig. 2**(a)**, the degradation of SMT was obviously suppressed in the present of L-histidine (L-his) (a typical inhibiting agent for $^1O_2$) [41], and the removal efficiency dropped from 91.4% to 26.1%, proving the significant role of $^1O_2$ in the elimination of SMT. In addition, for the sake of excluding the mechanism of non-radicals pathway in the form of electron transfer in nZVIC/PAA system, potassium dichromate ($K_2Cr_2O_7$) was chosen as the a quencher [42]. As shown in Fig. S15, SMT degradation in the nZVIC/PAA system was not substantially inhibited in the presence of $K_2Cr_2O_7$, which indicated that the electron transfer was negligible in the reaction system. Generally, Cu(III) could be produced through the electron transfer from Cu(II) to peroxides under the neutral to alkaline conditions in the Fenton-like process (Eq. (27)) [10]. For the benefit of gaining more credible evidence, using periodate as a stabilizer, which could react with Cu(III) to form a stabilized Cu(III)-periodate complex with a characteristic wavelength at 415 nm [43]. Nevertheless, the contribution of Cu (III) in the nZVIC/PAA system could be ruled out due to the absence of characteristic wavelength at 415 nm (Fig. S16). Moreover, it was reported that $Fe^{IV}O^{2+}$ may exist in PAA-AOPs in the presence of Fe^{2+} (Eqs. (28–29)) [44]. The yield of $PMSO_2$ (i.e., $\eta(PMSO_2)$, the molar ratio of $\Delta[PMSO_2]$ and $\Delta[PMSO]$) transformed from PMSO was measured to verify whether $Fe^{IV}O^{2+}$ was generated in the nZVIC/PAA system. As can be seen from Fig. S17, the yield of PMSO switched to $PMSO_2$ during the reaction was less than 5.0%, which indicated that the role of $Fe^{IV}O^{2+}$ in the nZVIC/PAA system could be negligible.

$$Fe^{2+} + CH_3C(O)OOH \rightarrow Fe^{3+} + CH_3C(O)O^{\bullet} + OH^- \quad (7)$$

$$Fe^{2+} + CH_3C(O)OOH \rightarrow Fe^{3+} + CH_3C(O)O^- + {}^{\bullet}OH \quad (8)$$

$$Fe^{3+} + CH_3C(O)OOH \rightarrow Fe^{2+} + CH_3C(O)OO^{\bullet} + H^+ \quad (9)$$

$$Cu^+ + CH_3C(O)OOH \rightarrow CH_3C(O)O^- + {}^{\bullet}OH + Cu^{2+} \quad (10)$$

$$Cu^+ + CH_3C(O)OOH \rightarrow CH_3C(O)O^{\bullet} + OH^- + Cu^{2+} \quad (11)$$

$$Cu^{2+} + CH_3C(O)OOH \rightarrow CH_3C(O)O^{\bullet} + H^+ + Cu^+ \quad (12)$$

$$CH_3C(O)O^{\bullet} \rightarrow {}^{\bullet}CH_3 + CO_2 \quad (13)$$

$$^{\bullet}CH_3 + O_2 \rightarrow CH_3(O)O^{\bullet} \quad (14)$$

$$CH_3C(O)OOH + {}^{\bullet}OH \rightarrow CH_3C(O)OO^{\bullet} + H_2O \quad (15)$$

$$CH_3C(O)OOH + CH_3C(O)O^{\bullet} \rightarrow CH_3C(O)OO^{\bullet} + CH_3COOH \quad (16)$$

$$Mn^{2+} + ROO^{\bullet} \leftrightarrow ROOMn^{3+} \quad (17)$$

$$CH_3C(O)OOH + {}^{\bullet}OH \rightarrow CH_3C(O)OH + HO_2^{\bullet} \quad (18)$$

$$HO_2^{\bullet} \leftrightarrow O_2^{\bullet-} \text{ (pH dependent)} \quad (19)$$

$$O_2^{\bullet-} + {}^{\bullet}OH \rightarrow OH^- + {}^1O_2 \quad (20)$$

$$O_2^{\bullet-} + HO_2^{\bullet} \rightarrow HO_2^- + {}^1O_2 \quad (21)$$

$$HO_2^- + H_2O_2 \rightarrow H_2O + OH^- + {}^1O_2 \quad (22)$$

$$HO_2^{\bullet} \rightarrow H^+ + {}^1O_2 \quad (23)$$

$$HO_2^{\bullet} + HO_2^{\bullet} \rightarrow H_2O + {}^1O_2 \quad (24)$$

$$2\ O_2^{\bullet-} + 2\ H_2O \rightarrow 2OH^- + H_2O_2 + {}^1O_2 \quad (25)$$

$$CH_3C(O)OOH + CH_3C(O)OO^- \rightarrow CH_3C(O)OH + CH_3C(O)O^- + {}^1O_2 \quad (26)$$

$$Cu(II) + H_2O_2 \rightarrow Cu(III) + {}^{\bullet}OH \quad (27)$$

$$Fe^{2+} + CH_3C(O)OOH \rightarrow CH_3C(O)OH + Fe^{IV}O^{2+} \quad (28)$$

$$Fe^{2+} + H_2O_2 \rightarrow H_2O + Fe^{IV}O^{2+} \quad (29)$$

In order to further prove the dominant species of ROS in the nZVIC/PAA system, the ESR detection was employed to detect the generated $^{\bullet}OH$/R-O$^{\bullet}$/$O_2^{\bullet-}$ and $^1O_2$ through the employment of DMPO and TEMP as the spin-trapping agents, respectively. As expected, the signals of DMPO-R-O$^{\bullet}$, DMPO-$^{\bullet}OH$ and DMPO-$O_2^{\bullet-}$ were detected, with the signal of DMPO-RO$^{\bullet}$ being the most intense, which was consistent with the results of the quenching experiments (Fig. 2**(b-c)**). As denoted in Fig. 2 (d), the signal of TEMP-$^1O_2$ in H_2O was also detected and the signal intensity increased with reaction time. This was consistent with the quenching experiment of $^1O_2$. Because the $^1O_2$ was sensitive to the physical quenching of H_2O and the short lifetime of $^1O_2$ in H_2O (2 μs), deuterium oxide (D_2O) (20–32 μs) was used to supersede H_2O to prolong the lifetime of $^1O_2$ in nZVIC/PAA system [45]. It can be seen from the ESR detection results that the signal of TEMP-$^1O_2$ trapped in D_2O was significantly stronger than the corresponding signal in the ultrapure water. Accordingly, $^1O_2$ was indeed produced and participated on the elimination of SMT in the nZVIC/PAA system. The source of $^1O_2$ was composed of two parts, one was the self-decomposition of PAA (Eq. (26)), and the other was the conversion of $O_2^{\bullet-}$ and $^{\bullet}OH$ produced by the system (Eqs. (20–25)). The radical quenching experiments, PMSO-based probe experiment, and ESR detection collectively demonstrated that radicals (R-O$^{\bullet}$, $^{\bullet}OH$, and $O_2^{\bullet-}$) and non-radical ($Fe^{IV}O^{2+}$ and $^1O_2$) were generated in the nZVIC/PAA system, and the $CH_3C(O)OO^{\bullet}$ and $^1O_2$ played a leading role on the removal of SMT. Furthermore, the contribution of $^{\bullet}OH$, $^1O^2$, and R-O$^{\bullet}$ to SMT removal was quantitatively assessed by kinetic experiments utilizing different probe compounds (i.e., *p*-chlorobenzoic acid (*p*-CBA), furfuryl alcohol (FFA), and naproxen (NPX)) [20,46]. The contribution of $^{\bullet}OH$, $^1O_2$, and R-O$^{\bullet}$ to SMT degradation in the nZVIC/PAA system were determined to be 7.8%, 33.0%, and 59.2%, respectively (Fig. 2(e) and Text S4). Therefore, the above

results was rapport with the quenching experiments and ESR detection, which was $^1O_2$ and R-O$^•$ dominate the SMT removal in the nZVIC/PAA process.

3.3.2. The synergy between Fe and Cu

In an effort to further analyze the mechanism of the SMT degradation in the nZVIC/PAA system, XPS analysis of the material of nZVIC before and after the oxidation reaction was carried out. It was reported that the redox cycle between Cu^+ and Cu^{2+} could promote the electron transfer and the Fe^{2+}/Fe^{3+} cycle [47]. As observed from Fig. 3(a-b), the XPS spectrum of the nZVIC after reaction still contained of Fe^0 and Cu^0, but the intensity was weakened, which indicated that Fe^0 and Cu^0 were partly consumed in the process of PAA activation to degrade SMT, while the existence of Cu might slow down the oxidation of Fe. The XPS spectrum of Fe 2p of original nZVIC with binding energy at 706.9 eV corresponded to the Fe^0 [48]. After the reaction, the binding energy of Fe^0 and Fe^{2+} were weakened, and the binding energy of Fe^{3+} appeared in the XPS spectrum of Fe 2p, which indicated that Fe^{2+} was oxidized to Fe^{3+} during the process. The proportion of Fe^{2+} decreased from 79.3% to 17.7%, while that of Fe^{3+} increased from 16.1% to 81.4%, which indicated that the co-existence and conversion of Fe^{2+}/Fe^{3+} in the reaction process. Meanwhile, it can be obtained from Fig. 3b that the XPS spectrum of Cu 2p of the original nZVIC had two peaks at 952.0 eV and 933.2 eV, which was geared to Cu^0 [21]. This result verified that Cu^0 was successfully formed in the synthesized nZVIC through the displacement method. In addition, the other four peaks at 933.8 eV, 940.9 eV, 943.2 eV, and 953.5 eV belonged to Cu^{2+} [34]. After the reaction, the XPS spectrum of Cu 2p showed two peaks attributed to Cu^+ at 932.8 eV and 952.5 eV [18], and the content of Cu^{2+} (Cu^0) was descended from 76.7% (23.3%) to 75.2% (18.3%) accompanied by the Cu^+ content raising, which indicated that the transformation of Cu^0 loaded on the surface of Fe^0 during the reaction. The appearance of Cu^+ strongly proved the electron transfer between Cu^{2+}/Cu^+, and further confirmed that the existence of redox cycles of Cu^{2+}/Cu^+ and Fe^{3+}/Fe^{2+} in the nZVIC/PAA process (Eq. (30)) [27], which was consistent with the previous reports [18,49].

$$Cu^+ + Fe^{3+} \rightarrow Cu^{2+} + Fe^{2+} \quad (30)$$

The Tafel diagrams of nZVIC and nZVI were tested, and the results were depicted in Fig. 3(c). nZVIC had a superior corrosion current (1.6×10^{-6} A) compared to the nZVI (2.7×10^{-7} A), indicating that the nZVIC had a faster electron transfer rate and more excellent catalytic activity than that of nZVI. This may be due to Cu loading on the surface of nZVI enhanced the reactivity of nZVI and thus improved the corrosion rate. Furthermore, the electrochemical impedance spectroscopy (EIS) test (Fig. 3(d)) proved that nZVIC had a smaller semicircular diameter than nZVI, which meant that nZVIC had a higher charge transfer efficiency and conductive properties [41]. Therefore, the electrochemical analysis further confirmed the superiority of nZVIC over nZVI, and owing to the bimetallic synergistic effect, nZVIC could effectively activate PAA to remove SMT under neutral conditions. In addition, in order to explore the main active sites of nZVIC in activating PAA, using NCP to complex with Cu on the surface of nZVIC for hindering electron transfer to the PAA [50]. As shown in Fig. S19, the removal efficiency of SMT reduced from 91.4% to 28.6% in the presence of NCP, indicating Fe^{2+} could activate PAA. Moreover, ZVC (without doping Fe) was used to activate PAA for the degradation of SMT, and only about 15.0% of SMT was removed by ZVC/PAA system after 20 min of reaction, which also illustrated that the activation effect of Cu on PAA was not good (Fig. S19). Besides, combined with the obvious changes of Fe^{2+} content before and after reaction in XPS spectrum, the main active sites of nZVIC in the activation of PAA should be Fe, but the existence of Cu was very important for the regeneration of Fe^{2+} on the surface of nZVIC.

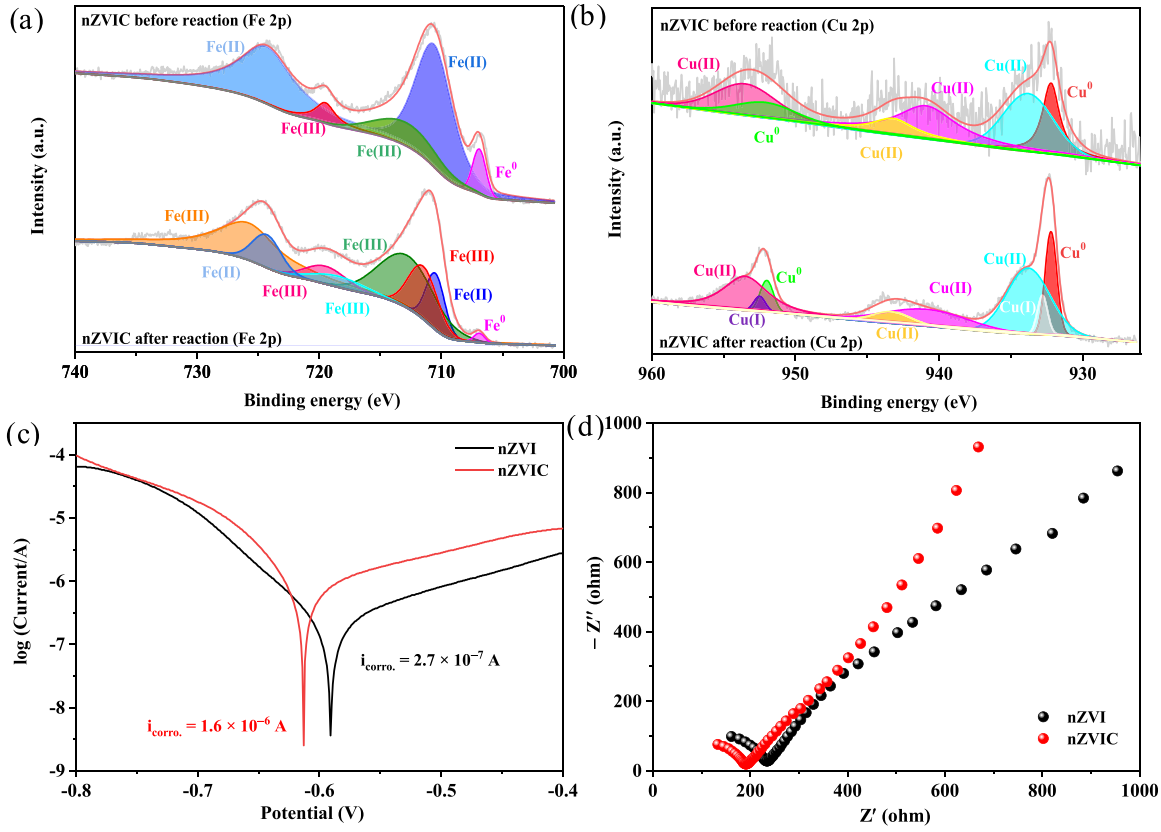

Fig. 3. XPS spectra of (a) Fe 2p and (b) Cu 2p of nZVIC before and after reaction, (c) Tafel polarization curves, and (d) electrochemical impedance spectroscopic analysis of the synthesized nZVIC and nZVI.

3.3.3. The DFT calculation and determination of intermediates

To better explore the mechanism of SMT degradation, it is necessary to determine the degradation intermediates of SMT and deduce its main degradation pathway in the nZVIC/PAA process. Therefore, for the benefit of investigating the degradation pathway of SMT in nZVIC/PAA system, the reactive sites of SMT were predicted via DFT theoretical calculation (**Text S3**) and the intermediate products of SMT were corroborated on account of the LC-MS analysis. The optimized molecular structure, the HOMO and LUMO orbital distribution of SMT were exhibited in Fig. S20. Fukui index (f^- and f^0 represent electrophilic and radical attack, respectively) is an important indicator to estimate the reactive sites on contaminants, and the results of Fukui function mapped electron density isosurface and dual descriptor map were presented in Fig. 4. The amino group N7 on the benzene ring had a large $f^-(r)$, which indicated that these sites were vulnerable to be attacked by electrophile and initiated the electrophilic reaction. The sites of C8, C13, and C14 on the benzene ring were also correspondingly susceptible to attack by the electrophile. According to previous studies, the non-radical $^1O_2$ and the radicals R-O$^\bullet$ and $^\bullet$OH generated in the AOPs could be considered as electrophiles, which were more preferred to attack the electrophilic sites of the pollutants [39,51,52]. Similarly, the dark blue color near the N5, N6, C15, and C16 on the pyrimidine ring corresponds to the most likely active site in the nucleophilic reaction (Fig. 4b). As can be seen from Fig. 4**c**, the isosurface map of $f^0(r)$ revealed that the pyrimidine ring and the amino group N7 on the benzene ring were vulnerable to be attacked by free radicals. The isosurface maps showed that the reactivity of pyrimidine and benzene rings on SMT was higher than that of sulfonamide group, and the reaction was more likely to occur at these sites. The dual descriptor could synchronously consider the reactions of electrophilic and nucleophilic without inspecting $f^-(r)$ and $f^+(r)$, respectively [53]. It can be obtained from Fig. 4**d** that the amino N7 and the C8, C13, and C14 on the benzene ring regions demonstrated large negative values, which indicated that these regions have a higher electrophilic reactivity, which was consistent with the conclusion of Fukui function. Furthermore, the calculation results of the corresponding Fukui function and dual descriptor were detailed in Table 1 and **S3**. The condensed dual descriptors (CDD) values of N7, C8, C14, C13, and C10 were negative and increased from small to large, which indicated that these atoms tend to undergo electrophilic reactions. This result was consistent with the maximum positive value of f^- (N7 > C8 > C13 > C14 > C12), which reflected that the uniformity of the calculation results acquired with the two methods. Furthermore, the Wiberg bond order is an important index of the bond cleavage and bond strength [54,55]. For the same type chemical bonds, the chemical bond with a smaller value of Wiberg bond order always meaning the low bond energy and easily cleavage [56]. As described in Fig. S21, the Wiberg bond orders in the skeleton of SMT molecule showed that the S1-C8 bond and S1-N4 bond on the sulfamide group had the smallest bond orders, which indicated that the breakage was most likely to occur at S1-C8 bond and S1-N4 bond. In addition, the N4-C11 bond was also susceptible to break during oxidation due to its relatively weak value of Wiberg bond order.

The chemical formula, *m/z*, and molecular structure of the detected degradation intermediates were provided in Table S4, and the gained MS spectra were shown in Fig. S22. According to the detected degradation intermediates and the DFT calculation results, the degradation pathway of SMT in nZVIC/PAA process was proposed, as summarized in Fig. 5(a). DFT calculation revealed that the C15, C16, and N5 atoms within the pyrimidine ring were highly vulnerable to R-O$^\bullet$ and $^\bullet$OH attack, due to the high f^0 values of 0.0644, 0.581, and 0.0579, respectively. Therefore, the intermediate of P1 (4-amino-*N*-carbamimidoylbenzenesulfonamide, *m/z* 215) was obtained by opening ring reaction through radical attack on the reactive site on the pyrimidine ring. The intermediate generated by SO_2 extrusion was triggered by the electrophilic attack of aniline group, so the intermediate of P1–1 (N^1-(4,6-dimethylpyrimidin-2-yl)benzene-1,4-diamine, *m/z* 215) could be attributed to the attack of N_7 of aniline group [53]. The intermediates of P3 (2-amino-2-((4-aminophenyl)sulfonamido)acetic acid, *m/z* 246) and P4 (2-(hydroxyamino)pyrimidine-4,6-dicarboxylic acid, *m/z* 200) containing −COOH may be attributed to the attack of R-O$^\bullet$ (like $CH_3C(O)OO^\bullet$) on P1 and P1–1, respectively, which can indirectly prove the reaction of SMT and R-O$^\bullet$ [20]. Besides, the S-N bond cleavage of P3 occurred with the detection of P6 (hydrosulfonylbenzene, *m/z* 143), which was consistent with the above Wiberg bond order value of S1-N4 bond. In addition, the higher f^- value and the lower CDD value at C8, which indicated that it was easier to be attacked by electrophiles such as R-O$^\bullet$ and $^1O_2$, and then the opening ring reaction occurred on the benzene ring to produce the intermediate P2 (*N*-(4,6-dimethylpyrimidin-2-yl)methanesulfonamide, *m/z* 202). Subsequently, the C-N bond was cleaved due to the relatively small value of Wiberg bond order value to form P5 (2,4,6-trimethylpyrimidine, *m/z* 123). These

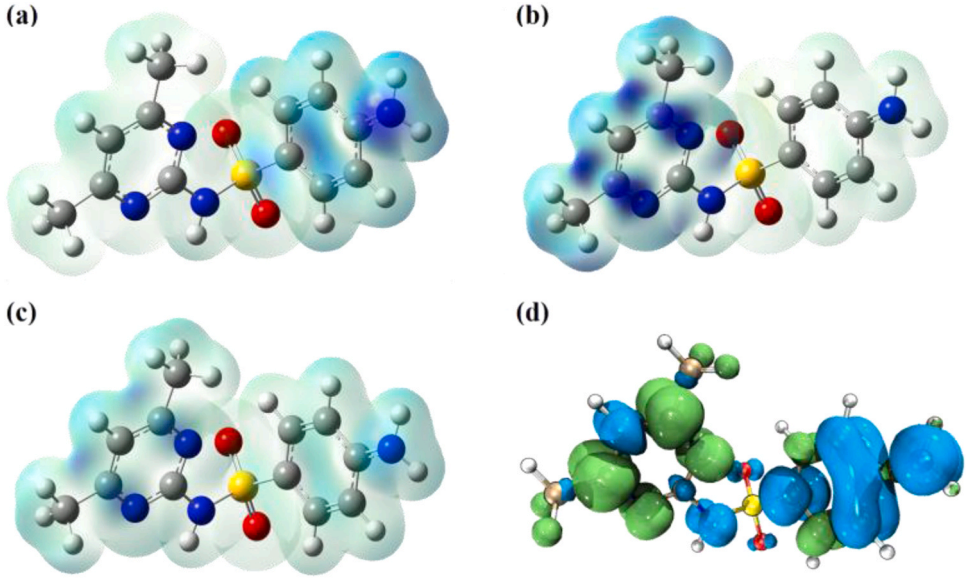

Fig. 4. The Fukui function mapped electron density isosurface (ρ = 0.01 a.u.): (a) f^-, (b)f^+, (c)f^0 (The dark blue on the isosurface denotes the larger positive value of the Fukui function), and (d) dual descriptor map (The isovalue is 0.002. Green and blue surfaces correspond to positive and negative regions, respectively). (For interpretation of the references to color in this figure legend, the reader is referred to the web version of this article.).

Table 1
Condensed Fukui function and dual descriptor of SMT.

No.	Atom	q (N)	q (N + 1)	q (N-1)	f^-	f^+	f^0	CDD
1	S	0.5186	0.5068	0.5346	0.016	0.0118	0.0139	-0.0042
2	O	-0.3362	-0.3676	-0.2966	0.0396	0.0314	0.0355	-0.0082
3	O	-0.3202	-0.3358	-0.2772	0.043	0.0156	0.0293	-0.0273
4	N	-0.1289	-0.1403	-0.0961	0.0328	0.0114	0.0221	-0.0214
5	N	-0.1888	-0.2831	-0.1672	0.0216	0.0943	0.0579	0.0727
6	N	-0.1662	-0.2572	-0.1711	-0.005	0.0911	0.0431	0.0961
7	N	-0.1709	-0.1871	-0.0346	0.1363	0.0162	0.0762	-0.1202
8	C	-0.0505	-0.0454	0.0373	0.0878	-0.005	0.0414	-0.0928
9	C	-0.0268	-0.0442	0.0104	0.0371	0.0175	0.0273	-0.0197
10	C	-0.0242	-0.019	0.0116	0.0359	-0.0052	0.0153	-0.0411
11	C	0.1511	0.1146	0.1502	-0.0008	0.0365	0.0178	0.0373
12	C	0.0584	0.0402	0.115	0.0566	0.0182	0.0374	-0.0383
13	C	-0.0637	-0.081	0.0031	0.0668	0.0174	0.0421	-0.0494
14	C	-0.064	-0.0762	0.0004	0.0644	0.0121	0.0383	-0.0523
15	C	0.0791	-0.0332	0.0956	0.0166	0.1123	0.0644	0.0957
16	C	0.0816	-0.0266	0.0896	0.008	0.1082	0.0581	0.1002
17	C	-0.0815	-0.1182	-0.05	0.0315	0.0367	0.0341	0.0052
18	C	-0.082	-0.1135	-0.0746	0.0074	0.0315	0.0194	0.0241
19	C	-0.0813	-0.1114	-0.077	0.0042	0.0302	0.0172	0.0259

intermediate products can be further oxidized by ROS in the reaction to smaller products and eventually converted to CO_2 and H_2O.

3.3.4. Toxicity evaluation

With the purpose of assessing potential risks of degradation products, the Toxicity Estimation Software Tool (T.E.S.T.) with the quantitative structure-activity relationship (QSAR) method was performed to evaluate the developmental toxicity, bioaccumulation factors, and mutagenicity of SMT and its degradation intermediates, and the results were displayed in Fig. 5**(b-c)** and Fig. S23. Except for the developmental toxicity of P1 and P2 was slightly higher than that of original SMT, the developmental toxicity of other intermediates was decreased, and P4 and P5 were even classified as "developmental non-toxicant", The bioaccumulation factors of P1, P3, and P5 were stronger than that of SMT, which may be due to their lipophilic structures [36]. The mutagenicity of most of the intermediates and SMT were negative. These results exhibited that the total actual toxicity of nZVIC/PAA/SMT reaction system was lower than before reaction after 20 min of treatment, but some intermediates should be given more attention due to their prediction still presented ecotoxicity. Furthermore, The acute toxicity of SMT degradation in the nZVIC/PAA system was assessed based on the standard method (UNE-EN-ISO 11348–3:2007(E)) by employing the BioFixLumi luminescent bacteria as an indicator [4,31], the details of procedure was exhibited in **Text S5**. As shown in Fig. S24, the inhibition rate of SMT against luminescent bacteria decreased from 58.7% to 37.3% after the reaction of nZVIC/PAA process. This result illustrated that the biotoxicity of SMT decreased with the progress of reaction in the nZVIC/PAA system.

3.3.5. The proposed reaction mechanism for SMT elimination

According to the discussion above and some previous studies, a possible mechanism responsible for the removal of SMT in nZVIC/PAA system was proposed in Scheme 1. Both homogeneous (minor) and heterogeneous (major) reactions were involved in the SMT elimination process in nZVIC/PAA system. In the preliminary stage, nZVIC transports Fe^{2+} and Cu^{+} to the surface of the material through the corrosion reaction (Eqs. (1–4)), while a small amount of ions are released into the solution. Then, Fe^{2+} and Cu^{+} on the surface activate PAA to generate ROS (e.g. $CH_3C(O)OO^{\bullet}$, $CH_3C(O)O^{\bullet}$, $^{\bullet}OH$, and $O_2^{\bullet-}$) (Eqs. (7–12)), which are oxidized to Fe^{3+} and Cu^{2+}. Besides, Fe^{2+} can also be oxidized by PAA to produce trace $Fe^{IV}O^{2+}$ (Eqs. (28–29)). $^{\bullet}OH$ and $O_2^{\bullet-}$ will be further converted to $^1O_2$ during the reaction (Eqs. (19–25)). Meanwhile, the loading of Cu not only enhances the electron transfer rate, but also greatly accelerates the transformation of Fe^{3+} to Fe^{2+} (Eq. (30)). Finally, these formed ROS would attack SMT and result in its degradation.

3.4. Effect of reaction parameters on SMT elimination

3.4.1. Effect of Fe/Cu mass ratio, nZVIC dose, and PAA concentration

The removal of SMT via nZVIC activated PAA with different Fe/Cu mass ratio was inspected. As depicted in Fig. 6**(a)**, the removal efficiencies of SMT in nZVIC/PAA system with the Fe/Cu mass ratio of 0 (nZVI), 3/1, 2/1, and 1/1 were 20.6%, 91.4%, 93.1%, and 88.1%, respectively, which demonstrated that the presence of Cu element obvious improved the performance of nZVI to activate PAA for the removal of SMT at neutral condition. With the increase of Cu loading, the degradation effect of SMT firstly increased and then decreased slightly, which might be owing to the excessive Cu loading would occupy the reactive sites on the surface of nZVI and hinder the reaction [57]. In addition, the nZVIC/PAA system with Fe/Cu mass ratio of 3/1 and 2/1 had almost the same removal efficiency on SMT. Considering the leaching of copper ions, the nZVIC with Fe/Cu mass ratio of 3/1 was selected for further study.

The effect of the dose of nZVIC on the elimination of SMT in nZVIC/PAA system was revealed in Fig. 6(b). The removal efficiency of SMT was enhanced from 15.3% to 91.4% with the dose of nZVIC increased from 10.0 mg L^{-1} to 50.0 mg L^{-1}, which was because the increase in the dose of nZVIC can provide more available reactive sites to activate PAA, thereby enhancing the removal efficiency of SMT [58]. Nevertheless, the removal efficiency of SMT was not continuously enhanced but decreased with nZVIC dose increased from 50.0 mg L^{-1} to 100.0 mg L^{-1}, which was reasonable to explain from two aspects. One was that excess nZVIC may compete with SMT for the reacted ROS [59], the other was that the excess Fe^{2+} released from nZVIC quenched the $^{\bullet}OH$ generated in the system [3]. Hence, the dose of nZVIC being 50.0 mg L^{-1} was selected for the elimination of SMT in this study.

The effect of PAA concentration on the removal of SMT in nZVIC/PAA system was given in Fig. 6**(c)**. With the increase of PAA concentration from 0.05 mM to 0.2 mM, the removal efficiencies of SMT increased correspondingly from 37.6% to 91.4%. This might be on account of the increase in PAA concentration, more ROS would be generated to remove SMT [60]. Nevertheless, when the concentration of PAA was further increased to 0.4 mM, the SMT removal was only slightly improved from 91.4% to 92.5%. Because the dose of the nZVIC was fixed, it meant that the number of reactive sites was certain. When excessive PAA was present in the reaction system, it cannot be completely activated by a limited catalyst to produce ROS to remove SMT [61]. Therefore, the concentration of PAA being 0.2 mM was selected for the SMT removal in this study by considering the economic issues and the utilization rate of PAA.

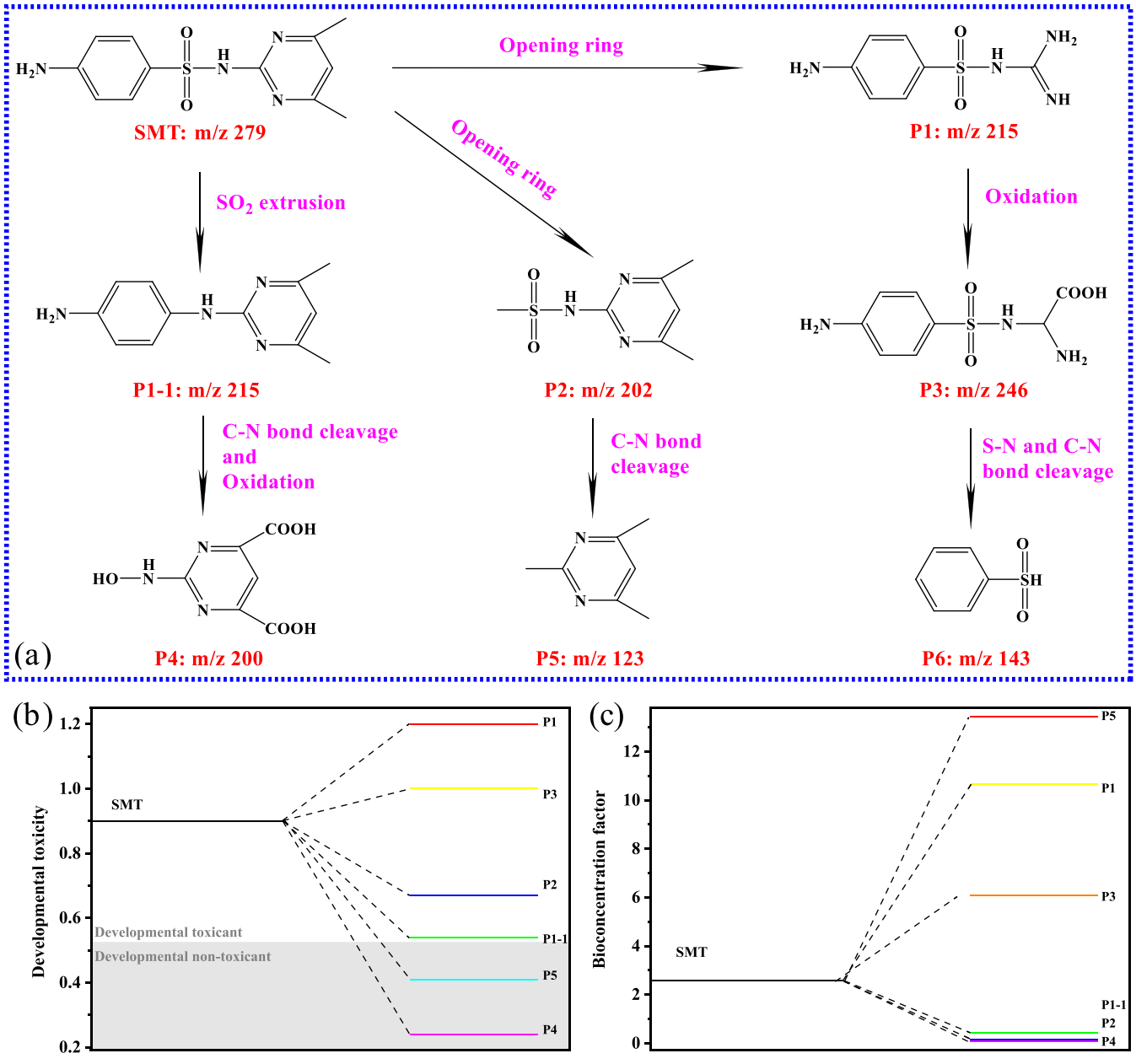

Fig. 5. (a) The possible degradation pathways of SMT in the nZVIC/PAA system. (b) The developmental toxicity, and (c) bioaccumulation factor of SMT and its possible degradation intermediate products.

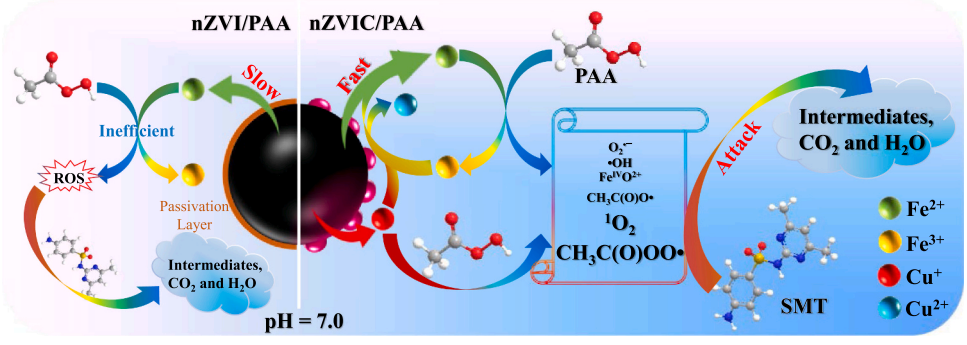

Scheme 1. The proposed mechanisms of SMT degradation in nZVIC/PAA system.

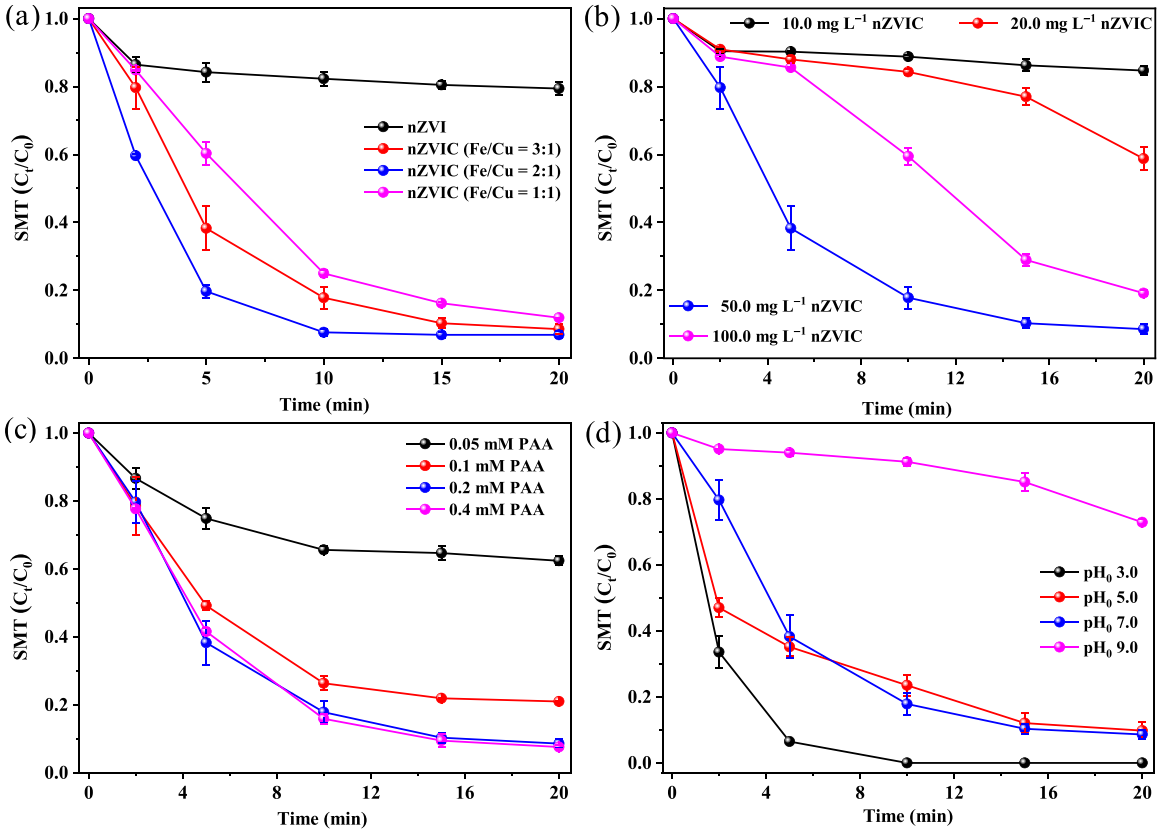

Fig. 6. Effect of (a) Fe/Cu mass ratio, (b) nZVIC dosage, (c) PAA concentration, and (d) initial pH on the degradation of SMT in nZVIC/PAA system. Reaction conditions: $[SMT]_0 = 10.0$ μM, $[nZVIC]_0 = 50.0$ mg L^{-1}, $[PAA]_0 = 0.2$ mM, $pH_0 = 7.0 \pm 0.1$, T = 25 ± 0.5 °C.

3.4.2. *Effect of initial pH*

The pH of the solution usually plays a momentous role in the process of AOPs, thus the effect of pH on the degradation of SMT in nZVIC/PAA system was investigated. It can be obtained from Fig. 6**(d)** that the removal efficiencies of SMT were all greater than 90.0% at pH 3.0, 5.0, and 7.0, wherein SMT was completely eliminated within 10.0 min at pH 3.0, whereas the removal efficiency was decreased to 27.2% at pH 9.0. This phenomenon indicated that nZVIC could effectively activate PAA to produce ROS for the oxidation of SMT in the pH range of 3.0–7.0. Moreover, the variation of pH at different pH in the nZVIC/PAA system during the reaction was measured and the result was shown in Fig. S25. Under different initial pH conditions, the change of pH could be neglected, because the variation was within 0.8 units during the reaction. Besides, the reason for the deteriorated removal efficiency of SMT at pH 9.0 might be as follows: When the pH was higher than 8.2, PAA existed mainly in the deprotonated form of (PAA^-), and the oxidation performance of PAA^- was weaker [2]. Furthermore, the point of zero charge (pH_{pzc}) of nZVIC was determined to be 4.3 by measuring the zeta potential (Fig. S26). The surface of nZVIC was negatively charged when the pH > 4.3. Therefore, the process of nZVIC activating PAA to generate ROS for SMT elimination would be inhibited due to the electrostatic repulsion effect between nZVIC and PAA at pH 9.0.

3.4.3. *Effect of inorganic anions and NOM*

The effects of common water matrices including inorganic anions (like Cl^-, SO_4^{2-}, and HCO_3^-) and natural organic matter (NOM, using humic acid (HA) as the representative of NOM) were further explored. The effects of Cl^- and SO_4^{2-} concentrations on SMT degradation by nZVIC/PAA were depicted in Fig. 7(a-b). It can be obtained that the existence of Cl^- and SO_4^{2-} had almost no effect on SMT elimination in nZVIC/PAA system, and this may be owing to the quenching effect of them on free radicals (e.g., $^{\bullet}OH$, R-O$^{\bullet}$) was very weak. However, the presence of HCO_3^- showed a negative effect on the removal of SMT in the nZVIC/PAA system. As illustrated in Fig. 7(c), with the HCO_3^- concentration increased from 0 to 2.0 mM, the removal efficiency of SMT dropped from 91.4% to 72.5%. According to the literature, HCO_3^- was a typical scavenger of $^{\bullet}OH$, but it had little effect to R-O$^{\bullet}$ [62]. Simultaneously, the pH of the solution after the addition of 2.0 mM HCO_3^- was measured. It was found that the pH increased from 7.0 to around 9.0 and then remained stable (Fig. S27). In addition, it could be seen from Fig. S28 that the decomposition of PAA was inhibited to some extent in the presence of HCO_3^-, which was coherent with the previous report [17]. Hence, the inhibition effect in the presence of HCO_3^- on the elimination of SMT in nZVIC/PAA process was mainly caused by the following two aspects: on the one hand, the solution pH was increased with the HCO_3^- added into the reaction system; on the other hand, the existence of HCO_3^- inhibited the decomposition of PAA. As shown in Fig. 7**(d)**, when the concentration of HA increased from 0 to 5.0 mg L^{-1}, the great reduction in the removal efficiency of SMT was observed, with a decrease from 91.4% to 18.5%. The obvious inhibition was primarily attributed to the complex of HA blocking the catalytic site and scavenging of R-O$^{\bullet}$ during the reaction [10,17].

3.5. *Practicability evaluation*

There were different water environments in nature, and the applicability of AOPs in different water samples was a quite important aspect of practical application. Therefore, the removal efficiency of SMT in different water samples (e.g., ultrapure water, river water, groundwater, and tap water) by nZVIC/PAA system was compared. As shown in Fig. 8 **(a)**, the removal efficiency of SMT was no obvious difference in different water samples, which was all around 90.0%, and the k_{obs} obtained in ultrapure water, river water, groundwater, and tap water were 0.1304, 0.1284, 0.1146, and 0.1112 min^{-1}, respectively (Fig. S29). This result

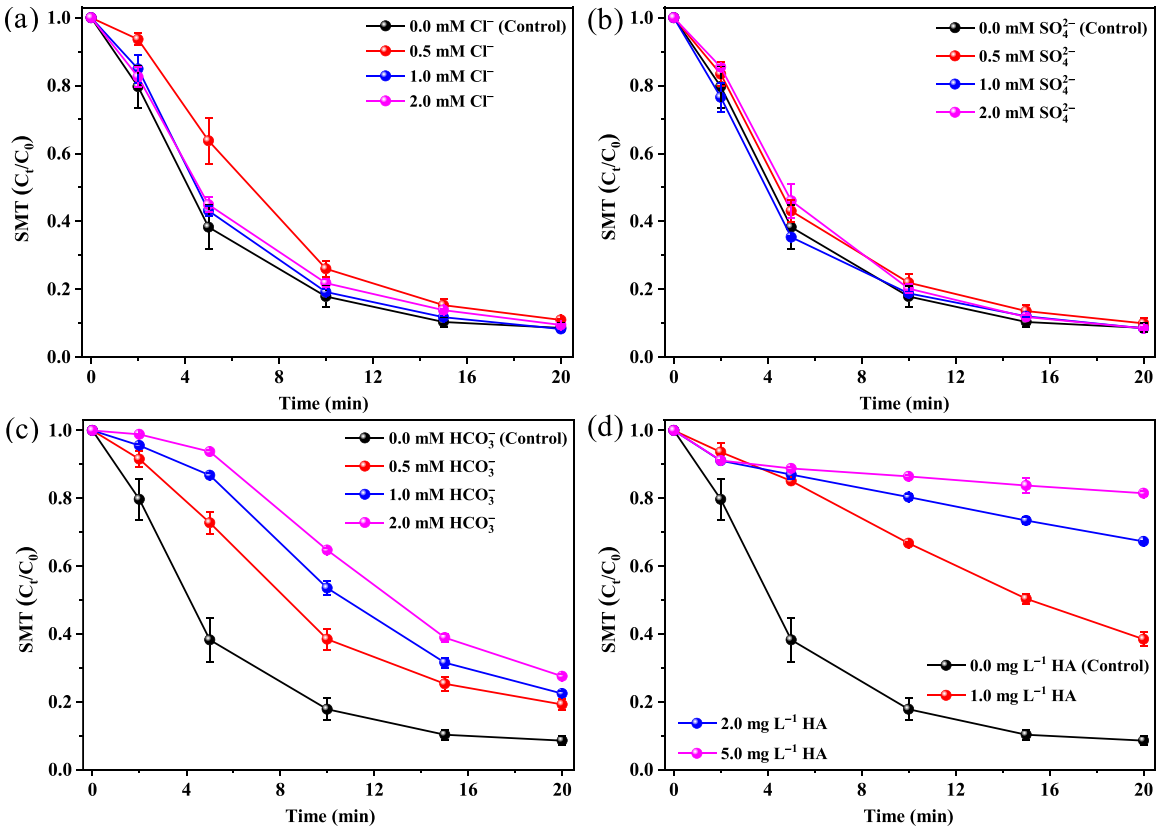

Fig. 7. Effect of the concentration of (a) Cl^-, (b) SO_4^{2-}, (c) HCO_3^-, and (d) humic acid on the degradation of SMT in nZVIC/PAA system. Reaction conditions: $[SMT]_0$ = 10.0 μM, $[nZVIC]_0$ = 50.0 mg L^{-1}, $[PAA]_0$ = 0.2 mM, pH_0 = 7.0 ± 0.1, T = 25 ± 0.5 °C.

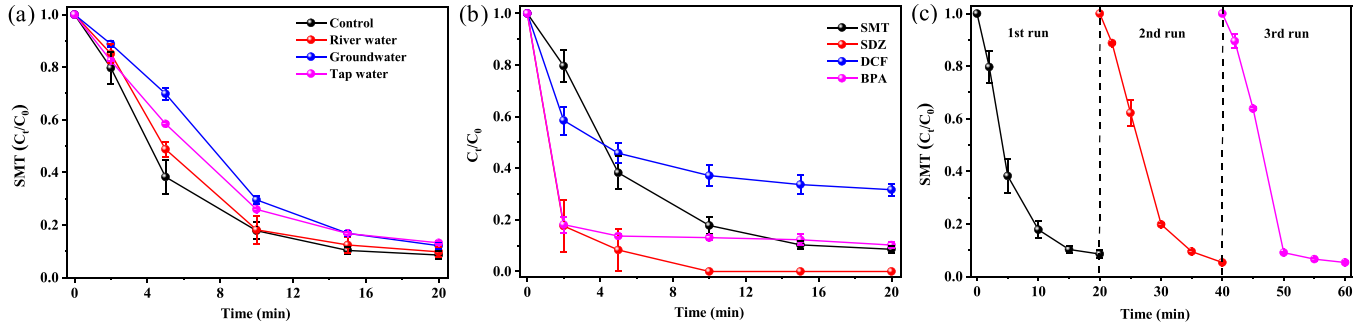

Fig. 8. (a) Degradation of SMT in different water samples in the nZVIC/PAA system. (b) The degradation of different pollutants in the nZVIC/PAA system. (c) Reusability of nZVIC in the nZVIC/PAA system for the degradation of SMT. Reaction conditions: $[SMT]_0$ = 10.0 μM, $[nZVIC]_0$ = 50.0 mg L^{-1}, $[PAA]_0$ = 0.2 mM, pH_0 = 7.0 ± 0.1, T = 25 ± 0.5 °C.

confirmed the universal applicability of the nZVIC/PAA system in different water samples. In addition, different contaminants such as sulfadiazine (SDZ), DCF, and bisphenol A (BPA) were selected to further evaluate the degradation performance of the nZVIC/PAA process. It could be seen from Fig. 8**(b)** that SDZ can be completely degraded within 10.0 min, and the removal efficiency of BPA could also be achieved to 89.7% during 20 min of reaction. This was on account of SDZ and BPA had electron-rich functional groups, which were more susceptible to be attacked by electrophilic ROS [29]. Nevertheless, nZVIC/PAA system could only remove 68.3% of DCF after 20 min, which demonstrated that the nZVIC/PAA system possessed selectivity towards contaminant degradation.

The reusability of nZVIC was awfully important for the practical application of nZVIC/PAA system. Hence, in the interest of evaluating the catalytic performance of the recovered nZVIC on PAA activation to remove SMT, three consecutive elimination of SMT were carried out by using the recovered nZVIC, and the results were displayed in Fig. 8**(c)**. The used nZVIC was collected with a magnet by utilizing the magnetic property, thoroughly washed with ultrapure water, and then vacuum dried. The removal efficiency of SMT was still higher than 90.0% during the third cycle when using nZVIC to activate PAA, which indicated that nZVIC was a recyclable and stable PAA activator. The favourable reusability of nZVIC for PAA activation might be owing to the presence of Cu in nZVIC, which promoted Fe^{2+}/Fe^{3+} interconversion (Eq. (23)). These results evidenced that nZVIC had an outstanding reusability in the nZVIC/PAA system for the elimination of SMT.

4. Conclusions

In the present work, a new strategy for the removal of SMT by

nZVIC/PAA process was proposed. With the selected experimental conditions, the nZVIC/PAA system could remove SMT up to 91.4% within 20 min, which was much higher than that of nZVI/PAA process (20.6%). The quenching experiments and ESR detection verified that there were many kinds of ROS (i.e., $^{\bullet}OH$, $O_2^{\bullet-}$, $CH_3C(O)OO^{\bullet}$, $CH_3C(O)O^{\bullet}$, $Fe^{IV}O^{2+}$, and $^1O_2$) in the system, among which $CH_3C(O)OO^{\bullet}$ and $^1O_2$ acted a dominant role in the elimination of SMT. The redox cycle of Fe^{2+}/Fe^{3+} could be accelerated by Cu loading on the surface of nZVIC, which benefited the continuous activation of PAA. The pathways of SMT degradation were proposed by DFT calculation and determination of intermediate products, the toxicity predictions of the intermediates were also performed via the QSAR method, and the acute toxicity of SMT during degradation was assessed by the luminescent bacteria test. The nZVIC/PAA system had good effectiveness on the degradation of SMT in a wide range of pH from 3.0–7.0. The presence of Cl^- and SO_4^{2-} showed a negligible effect on the removal of SMT, whereas HCO_3^- and HA greatly impeded SMT degradation in nZVIC/PAA system. In addition, according to the practicability evaluation (i.e., real water matrices, different pollutants, and cycle experiments), the nZVIC/PAA process was an innovative technology with great potential for practical water treatment.

CRediT authorship contribution statement

Junyang Xiao: Investigation, Writing – original draft. **Yangju Li:** Software, Writing – review & editing. **Haoran Dong:** Conceptualization, Methodology, Writing – review & editing, Supervision. **Zijun Pang:** Writing – review & editing. **Mengxi Zhao:** Writing – review & editing. **Daofen Huang:** Writing - Review & Editing. **Jie Dong:** Writing – review & editing. **Long Li:** Writing – review & editing.

Declaration of Competing Interest

The authors declare that they have no known competing financial interests or personal relationships that could have appeared to influence the work reported in this paper.

Acknowledgements

This research was supported by the National Natural Science Foundation of China (52122011), and the Science and Technology Innovation Program of Hunan Province (2021RC3050).

Supporting Information

Additional texts (Text S1-S5), tables (Table S1-S4), and figures (Figs. S1- S29) can be found on line.

Appendix A. Supporting information

Supplementary data associated with this article can be found in the online version at doi:10.1016/j.apcatb.2023.123183.

References

[1] H. Li, Y. Yang, X. Li, Z. Zhou, J. Feng, Y. Dai, X. Li, J. Ren, Degradation of sulfamethazine by vacuum ultraviolet-activated sulfate radical-advanced oxidation: efficacy, mechanism and influences of water constituents, Sep. Purif. Technol. 282 (2022), 120058, https://doi.org/10.1016/j.seppur.2021.120058.
[2] L. Yang, L. She, Z. Xie, Y. He, X. Tian, C. Zhao, Y. Guo, C. Hai, C. He, B. Lai, Boosting activation of peracetic acid by Co@mZVI for efficient degradation of sulfamethoxazole: Interesting two-phase generation of reactive oxidized species, Chem. Eng. J. 448 (2022), 137667, https://doi.org/10.1016/j.cej.2022.137667.
[3] L. Wang, J. Ye, J. Zhang, Q. Meng, X. Li, Z. Chen, H. Yu, A. Zhang, Z. Bu, Y. Jiao, Y. Pan, Removal of sulfamethazine using peracetic acid activated by Fe^0 and UV: Efficiency and mechanism study, J. Environ. Chem. Eng. 9 (2021), 106358, https://doi.org/10.1016/j.jece.2021.106358.
[4] H. Cai, J. Zou, J. Lin, J. Li, Y. Huang, S. Zhang, B. Yuan, J. Ma, Sodium hydroxide-enhanced acetaminophen elimination in heat/peroxymonosulfate system: production of singlet oxygen and hydroxyl radical, Chem. Eng. J. 429 (2022), 132438, https://doi.org/10.1016/j.cej.2021.132438.
[5] Y. Cheng, Z. Wang, J. Wang, L. Cao, Z. Chen, Y. Chen, Z. Liu, P. Xie, J. Ma, New insights into the degradation of micro-pollutants in the hydroxylamine enhanced Fe(II)/peracetic acid process: contribution of reactive species and effects of pH, J. Hazard. Mater. 441 (2023), 129885, https://doi.org/10.1016/j.jhazmat.2022.129885.
[6] Y. Li, H. Dong, J. Xiao, L. Li, D. Chu, X. Hou, S. Xiang, Q. Dong, Insights into a novel CuS/percarbonate/tetraacetylethylenediamine process for sulfamethazine degradation in alkaline medium, J. Hazard. Mater. 435 (2022), 128999, https://doi.org/10.1016/j.jhazmat.2022.128999.
[7] J. Xiao, S. Xiao, H. Dong, Z. Jin, Y. Li, L. Li, R. Tian, R. Li, J. Chen, Q. Xie, Degradation of sulfamethazine by amorphous zero-valent iron microspheres (A-mZVI) activated peroxydisulfate in groundwater, J. Clean. Prod. 346 (2022), 131276, https://doi.org/10.1016/j.jclepro.2022.131276.
[8] L. Zhang, J. Chen, T. Zheng, Y. Xu, T. Liu, W. Yin, Y. Zhang, X. Zhou, Co-Mn spinel oxides trigger peracetic acid activation for ultrafast degradation of sulfonamide antibiotics: Unveiling critical role of Mn species in boosting Co activity, Water Res (2022), 119462, https://doi.org/10.1016/j.watres.2022.119462.
[9] X. Ao, J. Eloranta, C. Huang, D. Santoro, W. Sun, Z. Lu, C. Li, Peracetic acid-based advanced oxidation processes for decontamination and disinfection of water: a review, Water Res 188 (2021), 116479, https://doi.org/10.1016/j.watres.2020.116479.
[10] J. Xiao, H. Dong, Y. Li, L. Li, D. Chu, S. Xiang, X. Hou, Q. Dong, S. Xiao, Z. Jin, J. Wang, Graphene shell-encapsulated copper-based nanoparticles (G@Cu-NPs) effectively activate peracetic acid for elimination of sulfamethazine in water under neutral condition, J. Hazard. Mater. 441 (2023), 129895, https://doi.org/10.1016/j.jhazmat.2022.129895.
[11] X. Ao, W. Wang, W. Sun, Z. Lu, C. Li, Degradation and transformation of norfloxacin in medium-pressure ultraviolet/peracetic acid process: An investigation of the role of pH, Water Res 203 (2021), 117458, https://doi.org/10.1016/j.watres.2021.117458.
[12] P. Du, J. Wang, G. Sun, L. Chen, W. Liu, Hydrogen atom abstraction mechanism for organic compound oxidation by acetylperoxyl radical in Co(II)/peracetic acid activation system, Water Res 212 (2022), 118113, https://doi.org/10.1016/j.watres.2022.118113.
[13] D. Xing, S. Shao, Y. Yang, Z. Zhou, G. Jing, X. Zhao, Mechanistic insights into the efficient activation of peracetic acid by pyrite for the tetracycline abatement, Water Res 222 (2022), 118930, https://doi.org/10.1016/j.watres.2022.118930.
[14] Y. Pan, Z. Bu, J. Li, W. Wang, G. Wu, Y. Zhang, Sulfamethazine removal by peracetic acid activation with sulfide-modified zero-valent iron: Efficiency, the role of sulfur species, and mechanisms, Sep. Purif. Technol. 277 (2021), 119402, https://doi.org/10.1016/j.seppur.2021.119402.
[15] J. Kim, T. Zhang, W. Liu, P. Du, J.T. Dobson, C. Huang, Advanced oxidation process with peracetic acid and Fe(II) for contaminant degradation, Environ. Sci. Technol. 53 (2019) 13312–13322, https://doi.org/10.1021/acs.est.9b02991.
[16] J. Xiao, R. Li, H. Dong, Y. Li, L. Li, S. Xiao, Z. Jin, Activation of sulfite via zero-valent iron-manganese bimetallic nanomaterials for enhanced sulfamethazine removal in aqueous solution:Key roles of Fe/Mn molar ratio and solution pH, Sep. Purif. Technol. 297 (2022), 121479, https://doi.org/10.1016/j.seppur.2022.121479.
[17] P. Zhang, X. Zhang, X. Zhao, G. Jing, Z. Zhou, Activation of peracetic acid with zero-valent iron for tetracycline abatement: The role of Fe(II) complexation with tetracycline, J. Hazard. Mater. 424 (2022), 127653, https://doi.org/10.1016/j.jhazmat.2021.127653.
[18] Q. Dong, H. Dong, Y. Li, J. Xiao, S. Xiang, X. Hou, D. Chu, Degradation of sulfamethazine in water by sulfite activated with zero-valent Fe-Cu bimetallic nanoparticles, J. Hazard. Mater. 431 (2022), 128601, https://doi.org/10.1016/j.jhazmat.2022.128601.
[19] Y. Li, X. Zhao, Y. Yan, J. Yan, Y. Pan, Y. Zhang, B. Lai, Enhanced sulfamethoxazole degradation by peroxymonosulfate activation with sulfide-modified microscale zero-valent iron (S-mFe^0): Performance, mechanisms, and the role of sulfur species, Chem. Eng. J. 376 (2019), 121302, https://doi.org/10.1016/j.cej.2019.03.178.
[20] Z. Xie, C. He, Y. He, S. Yang, S. Yu, Z. Xiong, Y. Du, Y. Liu, Z. Pan, G. Yao, B. Lai, Peracetic acid activation via the synergic effect of Co and Fe in CoFe-LDH for efficient degradation of pharmaceuticals in hospital wastewater, Water Res 232 (2023), 119666, https://doi.org/10.1016/j.watres.2023.119666.
[21] L. Zhang, Y. Fu, Z. Wang, G. Zhou, R. Zhou, Y. Liu, Removal of diclofenac in water using peracetic acid activated by zero valent copper, Sep. Purif. Technol. 276 (2021), 119319, https://doi.org/10.1016/j.seppur.2021.119319.
[22] J. Xiao, M. Wang, Z. Pang, L. Dai, J. Lu, J. Zou, Simultaneous spectrophotometric determination of peracetic acid and the coexistent hydrogen peroxide using potassium iodide as the indicator, Anal. Methods 11 (2019) 1930–1938, https://doi.org/10.1039/c8ay02772b.
[23] M. Kitis, Disinfection of wastewater with peracetic acid: a review, Environ. Int. 30 (2004) 47–55, https://doi.org/10.1016/S0160-4120(03)00147-8.
[24] L. Chekli, B. Bayatsarmadi, R. Sekine, B. Sarkar, A.M. Shen, K.G. Scheckel, W. Skinner, R. Naidu, H.K. Shon, E. Lombi, E. Donner, Analytical characterisation of nanoscale zero-valent iron: A methodological review, Anal. Chim. Acta 903 (2016) 13–35, https://doi.org/10.1016/j.aca.2015.10.040.
[25] E. Alp, The Facile Synthesis of Cu_2O-Cu hybrid cubes as efficient visible-light-driven photocatalysts for water remediation processes, Powder Technol. 394 (2021) 1111–1120, https://doi.org/10.1016/j.powtec.2021.09.031.
[26] W. Xiang, M. Huang, Y. Wang, X. Wu, F. Zhang, D. Li, T. Zhou, New insight in the O_2 activation by nano Fe/Cu bimetals: The synergistic role of Cu(0) and Fe(II),

Chin. Chem. Lett. 31 (2020) 2831–2834, https://doi.org/10.1016/j.cclet.2020.08.006.
[27] R. Yamaguchi, S. Kurosu, M. Suzuki, Y. Kawase, Hydroxyl radical generation by zero-valent iron/Cu (ZVI/Cu) bimetallic catalyst in wastewater treatment: Heterogeneous Fenton/Fenton-like reactions by Fenton reagents formed in-situ under oxic conditions, Chem. Eng. J. 334 (2018) 1537–1549, https://doi.org/10.1016/j.cej.2017.10.154.
[28] J. Wang, B. Xiong, L. Miao, S. Wang, P. Xie, Z. Wang, J. Ma, Applying a novel advanced oxidation process of activated peracetic acid by $CoFe_2O_4$ to efficiently degrade sulfamethoxazole, Appl. Catal. B Environ. 280 (2021), 119422, https://doi.org/10.1016/j.apcatb.2020.119422.
[29] L. Zhang, J. Chen, Y. Zhang, Z. Yu, R. Ji, X. Zhou, Activation of peracetic acid with cobalt anchored on 2D sandwich-like MXenes (Co@MXenes) for organic contaminant degradation: high efficiency and contribution of acetylperoxyl radicals, Appl. Catal. B Environ. 297 (2021), 120475, https://doi.org/10.1016/j.apcatb.2021.120475.
[30] R. Zhou, G. Zhou, Y. Liu, S. Liu, S. Wang, Y. Fu, Activated peracetic acid by Mn_3O_4 for sulfamethoxazole degradation: a novel heterogeneous advanced oxidation process, Chemosphere 306 (2022), 135506, https://doi.org/10.1016/j.chemosphere.2022.135506.
[31] Y. Huang, J. Zou, J. Lin, H. Yang, M. Wang, J. Li, W. Cao, B. Yuan, J. Ma, ABTS as both activator and electron shuttle to activate persulfate for diclofenac degradation: formation and contributions of $ABTS^{\bullet+}$, $SO_4^{\bullet-}$, and $^{\bullet}OH$, Environ. Sci. Technol. (2022), https://doi.org/10.1021/acs.est.2c04318.
[32] J. Kim, P. Du, W. Liu, C. Luo, H. Zhao, C. Huang, Cobalt/peracetic acid: advanced oxidation of aromatic organic compounds by acetylperoxyl radicals, Environ. Sci. Technol. 54 (2020) 5268–5278, https://doi.org/10.1021/acs.est.0c00356.
[33] R. Li, K. Manoli, J. Kim, M. Feng, C. Huang, V.K. Sharma, Peracetic acid–ruthenium (III) oxidation process for the degradation of micropollutants in water, Environ. Sci. Technol. 55 (2021) 9150–9160, https://doi.org/10.1021/acs.est.0c06676.
[34] L. Zhang, J. Chen, Y. Zhang, Y. Xu, T. Zheng, X. Zhou, Highly efficient activation of peracetic acid by nano-CuO for carbamazepine degradation in wastewater: The significant role of H_2O_2 and evidence of acetylperoxy radical contribution, Water Res 216 (2022), 118322, https://doi.org/10.1016/j.watres.2022.118322.
[35] X. Ao, X. Zhang, S. Li, Y. Yang, W. Sun, Z. Li, Comprehensive understanding of fluoroquinolone degradation via MPUV/PAA process: Radical chemistry, matrix effects, degradation pathways, and toxicity, J. Hazard. Mater. 445 (2023), 130480, https://doi.org/10.1016/j.jhazmat.2022.130480.
[36] Y. Li, H. Dong, L. Li, J. Xiao, S. Xiao, Z. Jin, Efficient degradation of sulfamethazine via activation of percarbonate by chalcopyrite, Water Res 202 (2021), 117451, https://doi.org/10.1016/j.watres.2021.117451.
[37] L. Wu, Z. Sun, Y. Zhen, S. Zhu, C. Yang, J. Lu, Y. Tian, D. Zhong, J. Ma, Oxygen vacancy-induced nonradical degradation of organics: critical trigger of oxygen (O_2) in the Fe–Co LDH/peroxymonosulfate system, Environ. Sci. Technol. 55 (2021) 15400–15411, https://doi.org/10.1021/acs.est.1c04600.
[38] Y. Jing, M. Jia, Z. Xu, W. Xiong, Z. Yang, H. Peng, J. Cao, Y. Xiang, C. Zhang, Facile synthesis of recyclable 3D gelatin aerogel decorated with MIL-88B(Fe) for activation peroxydisulfate degradation of norfloxacin, J. Hazard. Mater. 424 (2022), 127503, https://doi.org/10.1016/j.jhazmat.2021.127503.
[39] S. Li, Y. Yang, H. Zheng, Y. Zheng, C. He, B. Lai, J. Ma, J. Nan, Introduction of oxygen vacancy to manganese ferrite by Co substitution for enhanced peracetic acid activation and $^1O_2$ dominated tetracycline hydrochloride degradation under microwave irradiation, Water Res 225 (2022), 119176, https://doi.org/10.1016/j.watres.2022.119176.
[40] D.F. Evans, M.W. Upton, Studies on singlet oxygen in aqueous solution. Part 3. The decomposition of peroxy-acids, J. Chem. Soc. Dalton Trans. (1985) 1151–1153, https://doi.org/10.1039/dt9850001151.
[41] S. Xiang, H. Dong, Y. Li, J. Xiao, Q. Dong, X. Hou, D. Chu, Novel flower-like Fe-Mo composite for peroxydisulfate activation toward efficient degradation of carbamazepine, Sep. Purif. Technol. 305 (2023), 122487, https://doi.org/10.1016/j.seppur.2022.122487.
[42] Q. Guo, J. Xu, R. Tang, Y. Min, Z. Hu, P. Shi, Catalytic activation of peroxymonosulfate by Mn/N co-doped porous carbon for effective phenol degradation: crucial role of non-radical pathways, N. J. Chem. 47 (2023) 5420–5430, https://doi.org/10.1039/d3nj00340j.
[43] Y. Lei, C. Chen, Y. Tu, Y. Huang, H. Zhang, Heterogeneous degradation of organic pollutants by persulfate activated by CuO-Fe_3O_4: mechanism, stability, and effects of pH and bicarbonate ions, Environ. Sci. Technol. 49 (2015) 6838–6845, https://doi.org/10.1021/acs.est.5b00623.
[44] J. Lin, Y. Hu, J. Xiao, Y. Huang, M. Wang, H. Yang, J. Zou, B. Yuan, J. Ma, Enhanced diclofenac elimination in Fe(II)/peracetic acid process by promoting Fe (III)/Fe(II) cycle with ABTS as electron shuttle, Chem. Eng. J. 420 (2021), 129692, https://doi.org/10.1016/j.cej.2021.129692.
[45] B. Liu, W. Guo, W. Jia, H. Wang, Q. Si, Q. Zhao, H. Luo, J. Jiang, N. Ren, Novel nonradical oxidation of sulfonamide antibiotics with Co(II)-Doped g-C_3N_4-activated peracetic acid: role of high-valent cobalt–oxo species, Environ. Sci. Technol. 55 (2021) 12640–12651, https://doi.org/10.1021/acs.est.1c04091.
[46] Y. Li, H. Dong, J. Xiao, L. Li, D. Chu, X. Hou, S. Xiang, Q. Dong, Oxidation of sulfamethazine by a novel CuS/calcium peroxide/tetraacetylethylenediamine process: High efficiency and contribution of oxygen-centered radicals, Chem. Eng. J. 446 (2022), 136882, https://doi.org/10.1016/j.cej.2022.136882.
[47] Y. Ding, C. Pan, X. Peng, Q. Mao, Y. Xiao, L. Fu, J. Huang, Deep mineralization of bisphenol A by catalytic peroxymonosulfate activation with nano CuO/Fe_3O_4 with strong Cu-Fe interaction, Chem. Eng. J. 384 (2020), 123378, https://doi.org/10.1016/j.cej.2019.123378.
[48] W. Shen, F. Lin, X. Jiang, H. Li, Z. Ai, L. Zhang, Efficient removal of bromate with core-shell Fe@Fe_2O_3 nanowires, Chem. Eng. J. 308 (2017) 880–888, https://doi.org/10.1016/j.cej.2016.09.070.
[49] C. Fu, X. Yi, Y. Liu, H. Zhou, Cu^{2+} activated persulfate for sulfamethazine degradation, Chemosphere 257 (2020), 127294, https://doi.org/10.1016/j.chemosphere.2020.127294.
[50] Y. Ren, M. Shi, W. Zhang, D.D. Dionysiou, J. Lu, C. Shan, Y. Zhang, L. Lv, B. Pan, Enhancing the fenton-like catalytic activity of nFe_2O_3 by MIL-53(Cu) support: a mechanistic investigation, Environ. Sci. Technol. 54 (2020) 5258–5267, https://doi.org/10.1021/acs.est.0c00203.
[51] J. Duan, L. Chen, H. Ji, P. Li, F. Li, W. Liu, Activation of peracetic acid by metal-organic frameworks (ZIF-67) for efficient degradation of sulfachloropyridazine, Chin. Chem. Lett. 33 (2022) 3172–3176, https://doi.org/10.1016/j.cclet.2021.11.072.
[52] H. Ji, P. Du, D. Zhao, S. Li, F. Sun, E.C. Duin, W. Liu, 2D/1D graphitic carbon nitride/titanate nanotubes heterostructure for efficient photocatalysis of sulfamethazine under solar light: Catalytic "hot spots" at the rutile–anatase–titanate interfaces, Appl. Catal. B Environ. 263 (2020), 118357, https://doi.org/10.1016/j.apcatb.2019.118357.
[53] Y. Xie, J. Wan, Z. Yan, Y. Wang, T. Xiao, J. Hou, H. Chen, Targeted degradation of sulfamethoxazole in wastewater by molecularly imprinted MOFs in advanced oxidation processes: Degradation pathways and mechanism, Chem. Eng. J. 429 (2022), 132237, https://doi.org/10.1016/j.cej.2021.132237.
[54] I. Mayer, Bond order and valence indices: a personal account, J. Comput. Chem. 28 (2007) 204–221, https://doi.org/10.1002/jcc.20494.
[55] Z. Liu, Y. Fei, Z. Xia, R. Zhang, X. Chang, Y. Ji, D. Kong, J. Lu, J. Chen, Insights into the oxidation of bisphenol A by peracetic acid enhanced with bromide: the role of free bromine, Sep. Purif. Technol. 302 (2022), 122159, https://doi.org/10.1016/j.seppur.2022.122159.
[56] L. Shen, Z. Chen, J. Kang, P. Yan, J. Shen, B. Wang, S. Zhao, L. Bi, S. Wang, Y. Cheng, N-nitrosodimethylamine formation during oxidation of N,N-dimethylhydrazine compounds by peroxymonosulfate: Kinetics, reactive species, mechanism and influencing factors, J. Hazard. Mater. 428 (2022), 128191, https://doi.org/10.1016/j.jhazmat.2021.128191.
[57] B. Lai, Y. Zhang, Z. Chen, P. Yang, Y. Zhou, J. Wang, Removal of p-nitrophenol (PNP) in aqueous solution by the micron-scale iron–copper (Fe/Cu) bimetallic particles, Appl. Catal. B Environ. 144 (2014) 816–830, https://doi.org/10.1016/j.apcatb.2013.08.020.
[58] S. Xia, Z. Gu, Z. Zhang, J. Zhang, S.W. Hermanowicz, Removal of chloramphenicol from aqueous solution by nanoscale zero-valent iron particles, Chem. Eng. J. 257 (2014) 98–104, https://doi.org/10.1016/j.cej.2014.06.106.
[59] S. Yang, C. He, Z. Xie, L. Li, Z. Xiong, H. Zhang, P. Zhou, F. Jiang, Y. Mu, B. Lai, Efficient activation of PAA by FeS for fast removal of pharmaceuticals: The dual role of sulfur species in regulating the reactive oxidized species, Water Res 217 (2022), 118402, https://doi.org/10.1016/j.watres.2022.118402.
[60] W. Wu, D. Tian, T. Liu, J. Chen, T. Huang, X. Zhou, Y. Zhang, Degradation of organic compounds by peracetic acid activated with Co_3O_4: A novel advanced oxidation process and organic radical contribution, Chem. Eng. J. 394 (2020), 124938, https://doi.org/10.1016/j.cej.2020.124938.
[61] Q. Dong, Y. Li, J. Xiao, S. Xiang, X. Hou, D. Chu, Z. Zeng, H. Dong, Efficient catalytic degradation of sulfamethazine in aqueous solution by activation of peroxydisulfate with $CuFeO_2$, J. Environ. Chem. Eng. 11 (2023), 110564, https://doi.org/10.1016/j.jece.2023.110564.
[62] M. Cai, P. Sun, L. Zhang, C. Huang, UV/Peracetic acid for degradation of pharmaceuticals and reactive species evaluation, Environ. Sci. Technol. 51 (2017) 14217–14224, https://doi.org/10.1021/acs.est.7b04694.